

Dynamical tides excited in rotating stars of different masses and ages and the formation of close in orbits

S. V. Chernov^{1*}, J. C. B. Papaloizou^{2†} and P.B.Ivanov^{1‡}

¹ *Astro Space Centre, P.N. Lebedev Physical Institute, 84/32 Profsoyuznaya Street, Moscow, 117997, Russia*

² *DAMTP, Centre for Mathematical Sciences, University of Cambridge, Wilberforce Road, Cambridge CB3 0WA*

Accepted. Received; in original form

ABSTRACT

We study the tidal response of rotating solar mass stars, as well as more massive rotating stars, of different ages in the context of tidal captures leading to either giant exoplanets on close in orbits, or the formation of binary systems in star clusters. To do this, we adopt approaches based on normal mode and associated overlap integral evaluation, developed in a companion paper by Ivanov et al., and direct numerical simulation, to evaluate energy and angular momentum exchanges between the orbit and normal modes. The two approaches are found to be in essential agreement apart from when encounters occur near to pseudosynchronization, where the stellar angular velocity and the orbital angular velocity at periastron are approximately matched. We find that the strength of tidal interaction being expressed in dimensionless natural units is significantly weaker for the more massive stars, as compared to the solar mass stars, because of the lack of significant convective envelopes in the former case. On the other hand the interaction is found to be stronger for retrograde as opposed to prograde orbits in all cases. In addition, for a given pericentre distance, tidal interactions also strengthen for more evolved stars on account of their radial expansion. In agreement with previous work based on simplified polytropic models, we find that energy transferred to their central stars could play a significant role in the early stages of the circularisation of potential 'Hot Jupiters'.

Key words: hydrodynamics - celestial mechanics - planetary systems: formation, planet -star interactions, stars: binaries: close, rotation, oscillations

1 INTRODUCTION

Tidal interaction leads to synchronisation and orbital circularisation of close binary stars (eg. Zahn 1977, Hut 1981). It may also result in double star or star-planet systems that undergo close encounters in marginally unbound orbits becoming tidally captured into highly eccentric orbits that then begin to circularise (eg. Press & Teukolsky 1977). A process of this kind is believed to account for giant exoplanets in close orbits with periods of a few days (eg. Weidenschilling & Marzari 1996, Rasio & Ford 1996).

The determination of the tidal evolution requires the calculation of the response of the tidally perturbed body. This involves energy and angular momentum exchange between its normal modes and the orbit leading to its evolution. In a companion paper, Ivanov et al. (2013), subsequently referred to as Paper 1, we developed general pro-

cedures for calculating tidal energy and angular momentum exchange rates, for bodies in periodic orbits, that are associated with an identifiable regular spectrum of low frequency rotationally modified gravity modes, for rotating stars with realistic structure.

These are likely to give rise to the dominant tidal response in bodies with stratification, where the tidal forcing frequencies significantly exceed the inverse of the convective time scale associated with any convection zone, so that any effective turbulent viscosity is inefficient. This is also expected to be the case for rotating stars, when the dominant tidal forcing frequencies as viewed in the rotating frame exceed twice the rotation frequency with the consequence that inertial modes are not efficiently excited in convective regions.

In Paper 1 we also gave expressions from which the energy and angular momentum transferred to stellar modes of oscillation as a result of parabolic encounters can be calculated. A process that could lead to tidal captures and also governs the initial phase of orbital circularisation when the orbit is very eccentric (eg. Ivanov & Papaloizou 2004).

* E-mail: chernov@td.lpi.ru (SVCh)

† E-mail: J.C.B.Papaloizou@damtp.cam.ac.uk (JCBP)

‡ E-mail: pbi20@cam.ac.uk (PBI)

Evaluation of the response arising from normal modes requires calculation of mode eigenfrequencies and corresponding overlap integrals that determine the strength of mode coupling with the tidal potential (eg. Press & Teukolsky 1977). This procedure was discussed in some detail in Paper 1 for the case when the traditional approximation, appropriate for low frequency modes in stratified layers, was adopted. We remark that, as discussed in more detail in Paper 1, tidal phenomena such as energy and angular momentum exchange through parabolic encounters, or orbital evolution in the regime of so-called moderately strong viscosity (eg. Zahn 1977, Goodman & Dickson 1998), where propagating rotationally modified gravity waves attain short wavelengths, and so are dissipated before reaching boundaries from which they can be reflected, are such that results are independent of the precise specification of the dissipation process. In this regime, the wave dissipation should also occur on a time scale that is significantly longer than the locally excited wave period which will also be characteristic of the time for excitation due to tidal perturbation.

In this paper we apply the formalism developed in Paper 1, where only Sun-like stars were considered, to calculate the normal modes and their associated overlap integrals for a range of tidal forcing frequencies for two models of a rotating solar mass star with different ages, as well as several models of more massive rotating stars, with different ages. The dependence of these quantities on the existence and extent of convective regions and the transition between convective and radiative regions is elucidated. We also compare results obtained from the normal mode approach of Paper 1 to those obtained from direct numerical simulations of parabolic encounters (eg. Papaloizou & Ivanov 2010) delineating when there is good agreement between the two approaches. Our results are then applied to the tidal capture and initial orbital circularisation of giant exoplanets for both prograde and retrograde orbits and also the tidal capture of stars to form binary systems in stellar clusters (eg. Fabian, Pringle & Rees 1975, Press & Teukolsky 1977).

The plan of the paper is as follows. In section 2 we describe the stellar models for which we calculated the quantities that enable their exchange of energy and angular momentum under tidal gravitational perturbation due to a companion to be calculated. These quantities are the overlap integrals and the low frequency rotationally modified g mode spectrum and they are discussed in detail in Paper 1. We consider models in the range of $1-5M_{\odot}$ with a variety of ages. As indicated in Paper 1, the extent of any convective envelope and/or core plays a significant role in determining the strength of tidal interaction as also does the detailed form of the transition between convective and radiative regions.

In section 3 we discuss the properties of the numerically calculated mode spectra and overlap integrals for the stellar models considered. We also derive the rotational splitting coefficients which give the first order shifts of mode eigenfrequencies as a result of stellar rotation. In the non rotating case, the overlap integrals were found to be markedly larger for Sun-like stars as compared to either a polytrope with index 3 or more massive models with much less extensive convective regions. This is because of the convective envelope and is expected from the theory developed in Paper 1.

The overlap integrals are also calculated for rotating models under the neglect of centrifugal distortion and the adoption of the traditional approximation as indicated in Paper 1. Results for angular velocities of rotation in units of the critical rotation rate in the range $0.1-0.4$ are presented.

We go on to apply our results to evaluate the energy and angular momentum exchanged as a result of a parabolic encounter with a companion. These enable the possibility of tidal capture from unbound orbits to be assessed. In addition the time scale for the initial stages of orbital circularisation to occur for low planetary mass companions is estimated.

We compare energy and angular momentum transfers obtained through the normal mode/overlap integral approach to results obtained from solving the encounter problem as an initial value problem numerically (Papaloizou & Ivanov 2010; Ivanov & Papaloizou 2011) for the full range of rotation rates and for pericentre distances that are not too large to make calculation intractable. Both prograde and retrograde encounters are considered. We found that the methods are in good agreement apart from the situation where the system is close to pseudosynchronization. In this case the effective tidal forcing frequencies are comparable to the rotation frequency and inertial modes, not taken into account in the normal mode approach can play a significant role. As the characteristic tidal forcing frequencies are expected to be significantly larger than stellar rotation frequencies, inertial modes are unlikely to be excited in the star during the initial stages of the formation of close in giant planet orbits of ‘Hot Jupiters’. Accordingly we do not pursue the issue of inertial modes further in this paper.

Finally in section 5 we summarize and discuss our results. We remark that as in our earlier work (Ivanov & Papaloizou 2011), which considered polytropic models with index, 3, we find that tidal interaction with the central star is significantly stronger for retrograde orbits and that it could play a significant role in the circularisation process for giant planets, so potentially reducing the amount of potentially destructive energy dissipation in the planetary interior.

2 FORMULATION OF THE PROBLEM AND DETAILS OF NUMERICAL METHODS

2.1 Coordinate system and notation

The basic definitions and notation adopted in this paper are the same as in Paper 1. We use either a spherical coordinate system (r, ϕ, θ) or associated cylindrical polar coordinate system (ϖ, ϕ, z) with origin at the centre of mass of the star. When viewed in an inertial frame, the unperturbed star rotates uniformly about the z axis with angular velocity Ω . For our reference frame, we adopt the rotating frame in which the unperturbed star appears at rest.

2.2 Stellar models considered

Our calculations are for rotating stars of different masses and ages. As in paper 1 centrifugal distortion is neglected with the consequence that equilibrium structures are not modified by rotation. Therefore standard spherically symmetric models are used.

We consider models of stars of masses $M_* = 1, 1.5, 2,$

Model	Mass	Radius	Age	Mean density
1p	1	1		1
1a	1	0.91	$1.67 \cdot 10^8$	1.33
1b	1	1	$4.41 \cdot 10^9$	1
1.5a	1.5	2.08	$1.27 \cdot 10^7$	0.166
1.5b	1.5	1.46	$5.96 \cdot 10^7$	0.482
1.5c	1.5	1.82	$1.58 \cdot 10^9$	0.249
2a	2	2.68	$6.81 \cdot 10^6$	0.104
2b	2	1.63	$2.93 \cdot 10^7$	0.462
2c	2	2.25	$5.93 \cdot 10^8$	0.175
2d	2	2.91	$8.44 \cdot 10^8$	0.0811
5a	5	2.69	$2.54 \cdot 10^6$	0.257

Table 1. Radii, masses, ages and mean densities for models used in our calculations. Radii, masses and mean densities are expressed in units corresponding to the present day Sun, stellar ages are expressed in years.

and $5M_{\odot}$ of different ages. Stellar masses are expressed in solar masses ($1M_{\odot} = 1.9891 \cdot 10^{33} g$). Radii, R_* , are expressed in solar radii ($1R_{\odot} = 6.9551 \cdot 10^{10} cm$) and ages, expressed in years, are given in Table 1. Additionally, we have calculated all quantities of interest for a stellar model consisting of a polytrope with index $n = 3$. The mass and radius are scaled to solar values and the adiabatic index $\Gamma = 5/3$. This serves as reference model for our analysis and is referred to as model 1p.

All realistic stellar models apart from model 1b were kindly provided to us by I.W. Roxburgh. The numerical code used to obtain these models is discussed in Roxburgh (2008). Model 1b is for the present day Sun. It is discussed in Christensen-Dalsgaard et al. (1996). Unlike models described elsewhere in a similar context (see McMillan, McDermott & Taam 1987) our models have metallicity appropriate for population I stars. The zero age hydrogen mass fraction $X=0.7$ and the mass fraction of heavy elements $Z=0.02$ for all models.

Convective heat transport is described by a standard form of mixing length theory (Kippenhahn et al. 2013). Mixing in convective and semi-convective zones is dealt with by incorporating diffusion into the equations governing the evolution of the chemical abundances (see Eggleton 1972). The diffusion coefficient is taken to be $D_{conv} = v_{conv}l/6$, where v_{conv} is the convective velocity and l is the mixing length.

As is discussed in Paper 1 when low frequency gravity modes are considered, their important properties are found to be mainly determined by the functional forms of the density, ρ , and the Brunt - Väisälä frequency N . In particular, the locations of stably stratified radiative regions, where $N^2 > 0$, and the behaviour of N in the neighbourhood of transitions from stably stratified to convective regions, are particularly significant. For the models described here the functional forms in these transition regions are strongly affected by the evolutionary history of the chemical compo-

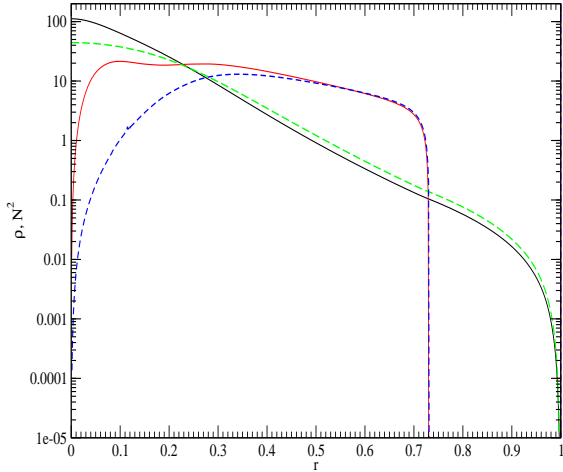


Figure 1. The density ρ (in units of the mean density $\bar{\rho} = 3M_*/(4\pi R_*^3)$) and square of the Brunt - Väisälä frequency, N^2 (in units of GM_*/R_*^3) as functions of the radius r expressed in units of R_* . The solid curves correspond to model 1b while the dashed curves are for the model 1a. The curves monotonically decreasing with r are for the density distributions, while the curves having maxima at some values of r are for the Brunt - Väisälä frequencies.

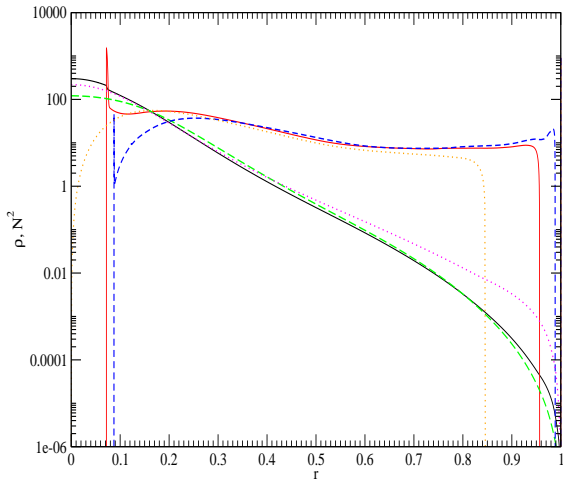


Figure 2. Same as in Fig. 1 but for models with $M_* = 1.5M_{\odot}$. Solid, dashed and dotted curves are for models 1.5c, 1.5b and 1.5a, respectively. Note that there are regions very close to the surface where a weak density inversion occurs in these models. However, the values of the density where this occurs are below the minimum level plotted.

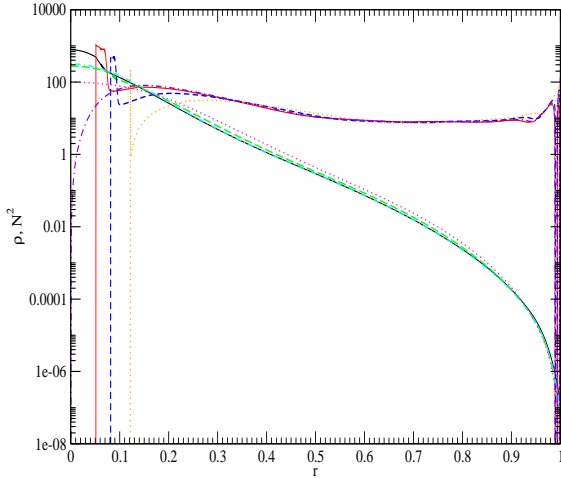


Figure 3. Same as in Fig. 1 but for models with $M_* = 2M_\odot$. Solid, dashed, dotted and dot-dashed curves are for models 2d, 2c, 2b and 2a, respectively. Note that the dashed and dot-dashed curves for the density almost coincide

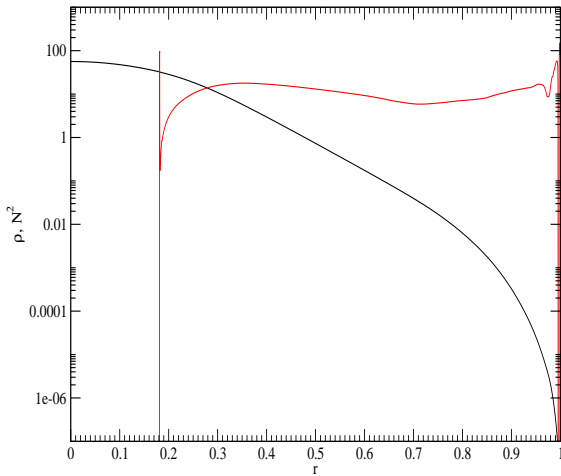


Figure 4. Same as in Fig. 1 but for model 5a with $M_* = 5M_\odot$.

sition profiles. Although chemical diffusion is included, the coefficient is zero in radiative regions and large in convective regions so that mixing is efficient there. This results in the possibility of very rapidly varying or even discontinuous abundance profiles according to how the boundary between a radiative and convective zone moves with evolution. Suppose this interface moves with speed v_I , we can form the

dimensionless quantity $v_I l / D_{conv} = 6v_I / v_{conv} \sim t_{conv} / t_{ev}$, the latter ratio being the ratio of the convection time scale to the evolutionary time scale.

On dimensionless grounds we might expect the width of the transition region, w_{rc} , between a convective and radiative zone would be given by an expression of the form $w_{rc} \sim l F(t_{conv} / t_{ev})$, where the form of the function F is determined by the way the diffusion coefficient vanishes as the radiative zone is entered and the evolutionary history. Simple modelling suggests that F is a monotonic function of its argument, with the variation being more rapid for diffusion coefficients with more rapid cutoffs. For example a linear variation is expected when the diffusion coefficient inside the radiative region vanishes as $(r - r_I)^2 / l^2$, with r_I being a distance of one mixing length away from a retreating convection zone boundary. Note that, $t_{conv} / t_{ev} \sim 10^{-(9-10)}$, is very small leading to the possibility of very thin transition layers when the evolutionary history is such that the composition in a convective zone differs significantly from its immediate surroundings. At such a transition the mean molecular weight changes while hydrostatic equilibrium enforces continuity of the pressure. There is then a rapid change in the density with an associated spike in the density gradient and the square of the Brunt-Väisälä frequency. As this results from the density gradient, a large effect can be produced with there being only small jumps in the density or chemical profile.

Plots of the density ρ and the square of the Brunt - Väisälä frequency, N^2 , against radius, for the models used in our calculations are given in Figs. 1-4. In Fig. 1 we illustrate these two quantities the two models with $M_* = 1M_\odot$ discussed in detail and adopted in Paper 1. Note that negative values of N^2 that occur in convective regions are not shown. These models exhibit a similar and rather simple structure. They have a radiative core and convective envelope with a transition at a similar total radius fraction. The young Sun-like star, model 1a, has a smaller radius than model 1b, which corresponds to the present day Sun. It accordingly has a larger mean density and is therefore, less susceptible to tidal influence from a perturbing companion with a given orbital period.

Models 1.5a-1.5c, illustrated in Fig. 2, are for a star of mass $M_* = 1.5M_\odot$ at different ages. Their structure is more complex than that of Sun-like stars. The youngest model 1.5a (plotted with dotted curves) is similar to models 1a and 1b in that it also has convective envelope with a convective core being absent. We remark that a weak density inversion occurs very close to the surface in these models. This is a well known effect that occurs as hydrogen is ionised in convective envelopes where the energy transport due to convection is inefficient (see eg. Latour 1970). The ionisation zone is very thin in such cases, and such that the reduction in the mean molecular weight, that occurs with weak pressure variation there, causes the density inversion. The density in these layers is very small and so they do not affect any of the tidal response calculations presented in this paper significantly. However, on account of the general similarity of the models, we expect that the overlap integrals, Q , characterising the strength of tidal interactions and discussed in detail in Paper 1, will have similar properties to those obtained for Sun-like stars. But, the density at the base of convection zone, expressed in terms of the mean density $\tilde{\rho} = 3M_* / (4\pi R_*^3)$, ρ_{cb} ,

is smaller than the corresponding quantity for models 1a and 1b. We find $\rho_{cb} \sim 10^{-3}\tilde{\rho}$ and $\sim 10^{-2}\tilde{\rho}$ for model 1.5a, and either of models 1a or 1b respectively.

The analytic WKBJ theory developed in Paper 1 predicts that the overlap integrals, being determined by the presence of a convective envelope, are proportional to $\sqrt{\rho_{cb}}$ in the limit of sufficiently small eigenfrequencies (see equations (111), (113) and (115) of Paper 1). Accordingly, we expect that for a given value of the eigenfrequency, Q values for model 1.5a will be smaller than those for younger models, by a factor corresponding to the square root of the ratio of the respective values of ρ_{cb} . Here we recall that as the mode spectrum is dense the overlap integrals are regarded as continuous functions of frequency. Let us note that energy and angular momentum exchanges due to tides associated with a normal mode are, in general, proportional to the square of the appropriate overlap integral (see Paper 1). That means that in a situation where the contribution from the convective envelope and the region of its boundary with the inner radiative zone determines the value of the overlap integral, energy and angular momentum exchanges are approximately proportional to ρ_{cb} , see also equation (13) of Goodman & Dickson (1998).

Our expectation is confirmed by calculation, see Fig. 8. The evolved models 1.5b and 1.5c have both convective envelopes and convective cores. However, ρ_c at the base of convective envelope is relatively small, being $\sim 4.6 \cdot 10^{-5}$ for model 1.5c and $\sim 6 \cdot 10^{-6}$ for model 1.5b. This has the consequence that the contribution to the overlap integrals associated with the presence of a convective envelope is strongly suppressed.

Models 1.5b and 1.5c also have convective cores. But, the transition region between the radiative region and the convective core is extremely sharp in these models (see discussion in Section 2.2 above), and must be considered as a discontinuity for eigenfunctions with characteristic wavelength larger than the typical size of the transition zone. The width of the latter, Δr , is of the order of or smaller than the grid size with $\Delta r/r < 2.5 \times 10^{-4}$, 2.5×10^{-5} for models 1.5b and 1.5c, respectively. We emphasise that the detailed form of this transition region should be determined from a complete treatment of convection, including overshoot, see eg. Roxburgh (1978), Zahn (1991), and the effects of stellar rotation, etc. This cannot be undertaken at present¹. However, when eigenfunctions have typical wavelengths larger than the size of the transition zone, one cannot assume that the Brunt - Väisälä frequency increases as a power of distance from the boundary of the convective region and perform a standard WKBJ analysis that assumes the response wavelength is significantly shorter than the transition width. Accordingly estimates of quantities characterising tidal interactions, such as overlap integrals or related quantities, for example the quantity E_2 used by Zahn (1977), based on this assumption are not valid.

Let us estimate typical periods of modes, where such calculations are potentially formally invalid. For definiteness

we consider model 1.5b. We assume that the width of the transition zone is as small as suggested by our numerical model. From Fig. 2 we see that for this model, the value of Brunt - Väisälä frequency at the maximum of the 'spike' close to the convective core is ≈ 6.8 and the radius of convective core $r_c \approx 0.087$ in our dimensionless units.

From the WKBJ theory applied to gravity waves, the characteristic wavelength, λ , can be estimated through $\lambda \approx r\omega/(\sqrt{6}N)$, where ω is the eigenfrequency and it is assumed that the star is non-rotating, see eg. Christensen-Dalsgaard (1998). On the other hand λ should be larger than the width of the transition region, estimated above as $\sim 2.5 \times 10^{-4}r$ or smaller. Thus we obtain $\omega > 4.2 \cdot 10^{-3}$ in natural units for this inequality to be valid. From table 1 it follows that this corresponds to periods < 40 days. This means that estimates based on a standard WKBJ analysis may be inapplicable for all periods of interest. Let us stress, however, that the width of the transition region may be much larger than was assumed in order to obtain this estimate (see discussion in Section 2.2).

In Fig. 3 we show the forms of the density and the square of Brunt - Väisälä frequency for models with $M_* = 2M_\odot$. The youngest model, model 2a (dot-dashed curve) is fully radiative. We expect that for this model, overlap integrals are suppressed at low frequencies as compared to models with convective regions. The overlap integrals associated with such models are expected to decrease with eigenfrequency, ω , faster than any power of ω , as happens for a polytropic star represented as model 1p. Thus, tidal interactions determined by low frequency gravity modes become rather inefficient in this case. Models 2b-2d are similar to those with mass $M_* = 1.5M_\odot$ with the difference that the convective envelope is practically absent. Therefore, contributions to the overlap integrals coming from the envelope region should be very small. There are also almost discontinuous transitions from radiative envelopes to convective cores. Thus we conclude that previous estimates of the strength of tidal interactions based on the regular behaviour of N^2 close to this transition may need revision.

Finally, in Fig 4 we plot the density and square of the Brunt - Väisälä frequency for a model of a young star with $M_* = 5M_\odot$. The structure of this model is rather simple and similar to the cases of evolved stars with $M_* = 2M_\odot$. There is no convective envelope in this model and, again, there is a quite sharp transition between the radiative region and convective core.

3 PROPERTIES OF STELLAR EIGENMODES: EIGENSPECTRA, OVERLAP INTEGRALS AND ROTATIONAL SPLITTING COEFFICIENTS

In this Section we consider the quantities that determine the tidal interactions for given orbital parameters and properties of decay of free stellar oscillation either due to viscosity or non-linear effects. These are the eigenfrequencies of free pulsations ω , normalised overlap integrals \tilde{Q} , and, in case of small rotational frequency $\Omega \ll \Omega_* \equiv \sqrt{GM_*/R_*^3}$, the coefficients β which determine the splitting of eigenfrequencies due to rotation in the non-rotating frame. We discuss how these quantities depend on stellar structure

¹ Note that future advances in astroseismology may lead to some observational constraints on details of transitions between radiative and convective regions in the near future, see eg. Silva Aguirre et al. (2011).

The overlap integrals are discussed in detail in Paper 1. Here we briefly recall them for completeness. In general, \hat{Q} is given by the expression

$$\hat{Q} = Q/\sqrt{n}, \quad Q = \left(\xi \left| \int_0^{2\pi} d\phi e^{-im\phi} \nabla(r^2 Y_2^m) \right| \right), \quad (1)$$

where it is implied that the inner scalar product of any two complex vectors $\boldsymbol{\eta}_1$ and $\boldsymbol{\eta}_2$ is determined by integration over the cylindrical coordinates ϖ and z as

$$(\boldsymbol{\eta}_1 | \boldsymbol{\eta}_2) = \int \varpi d\varpi dz \rho (\boldsymbol{\eta}_1^* \cdot \boldsymbol{\eta}_2), \quad (2)$$

Here $*$ denotes the complex conjugate, Y_2^m is the spherical function, $\boldsymbol{\xi}$ is the Lagrangian displacement vector corresponding to a particular eigenmode with eigenfrequency ω . It is assumed that in all expressions the dependence of $\boldsymbol{\xi}$ on the azimuthal angle ϕ , $\boldsymbol{\xi} \propto e^{im\phi}$, is factored out. In general the azimuthal mode number, m , is such that $|m| \leq 2$. However, we shall consider only $|m| = 2$ below as this is the most important case (see Paper 1).

The norm n is determined by the expression

$$n = \pi((\boldsymbol{\xi} | \boldsymbol{\xi}) + (\boldsymbol{\xi} | \mathcal{C}\boldsymbol{\xi})/\omega^2), \quad (3)$$

where \mathcal{C} is an integro-differential self-adjoint operator, which when operating on $-\boldsymbol{\xi}$ gives the restoring acceleration due to the action of gravity and pressure forces.

When the star is non-rotating the overlap integrals reduce to the form given by Press & Teukolsky (1977). A similar expression can be obtained in the so-called traditional approximation discussed below and in Paper 1. In that case we have

$$Q = \alpha Q_r, \text{ with } Q_r = \int_0^{R_*} r^3 dr \rho (2\xi + \Lambda \xi^S), \quad (4)$$

and $n = n_{st} + n_r$,

$$\text{where } n_{st} = \int_0^{R_*} r^2 dr \rho (\xi_j^2 + \Lambda (\xi^S)^2), \text{ and } n_r = \nu I_r I_\theta \quad (5)$$

with $I_r = \int_0^{R_*} r^2 dr \rho (\xi^S)^2$ and $\nu = 2\Omega/\omega$. In the expressions (4) and (5) $\xi(r)$ and $\xi^S(r)$ give the radial dependences of the radial component of the displacement vector and the angular components, respectively, in the traditional approximation. The quantities Λ , α and I_θ are functions of ν , their explicit form and the dependence on ν are discussed in Paper 1. Note that $\Lambda(\nu)$ is an eigenvalue associated with acceptable solutions of the Laplace tidal equation.

When the star does not rotate, the Laplace tidal equation reduces to the Legendre equation, the solution of which is the associated Legendre function. We then have $\alpha = 1$, $\Lambda = 6$, $n = n_{st}$ and the expressions (4) and (5) reduce to their standard form as given by e.g. Press & Teukolsky (1977) and Ivanov & Papaloizou (2004).

Hereafter we express all quantities of interest in natural units. Thus, eigenfrequencies are expressed in terms of the natural stellar frequency Ω_* , and the overlap integrals in terms of $\sqrt{M_*} R_*$.

3.1 Eigenfrequencies and overlap integrals for non-rotating stars

Let us first discuss the eigenfrequencies and overlap integrals for non-rotating models. In this case we set $\alpha_i = 1$ and $n_r = 0$ in (4) and (5), respectively. Eigenfrequencies, and eigenfunctions were obtained by a shooting method described in Section 5.2 of Paper 1. Here we note that we integrated the standard full set of four equations describing adiabatic pulsations (eg. Christensen-Dalsgaard 1998) to find these quantities for relatively large values of eigenfrequencies $\omega > 0.3 - 0.5$ depending on the particular model. These were then used to evaluate the overlap integrals. For smaller eigenfrequencies, the Cowling approximation is used to find the eigenfrequencies and the expression (78) of Paper 1 was employed to find the overlap integrals. This expression is equivalent to the original one presented above provided the Cowling approximation is used to find eigenmodes.

We checked that in the intermediate region for which $\omega \sim 0.3 - 0.5$ both methods give practically the same results. The advantage of using the expression (78) of Paper 1 in the low frequency limit is the fact that the integrand in this expression is less oscillatory in comparison to the integrand in the original expression, thus allowing us to significantly increase accuracy of determination of \hat{Q} in this limit where the eigenfunctions contain a large number of nodes.

Models of massive stars have very rapid variations of N^2 , see Figs 2-4 in the transition regions between radiative envelopes and convective cores. Since the characteristic radial extent of these variations can be of the order of the initial stellar model grid size a treatment of discontinuities may be needed. We prefer, however, to avoid this situation in our approach. To deal with this issue, we worked with computational grids which had a much larger number of grid points than were originally used to represent the structure of the stellar models. State variables were interpolated onto our more refined grid as smooth functions. There were then no discontinuities in the eigenfunctions on the refined grid, see Figs 5, 6.

The results of calculations of overlap integrals are shown in Figs. 7-10. In Fig. 7 we show the results for models 1p, 1a and 1b. Since the polytropic model 1p has been discussed extensively elsewhere (eg. Press & Teukolsky 1977, Lee & Ostriker 1986, Ivanov & Papaloizou 2004 and references therein) and overlap integrals corresponding to models 1a and 1b are discussed in detail in Paper 1, here we only mention that the polytropic model has much smaller overlap integrals when $\omega < 0.4$. This is due to the fact that \hat{Q} corresponding to Sun-like stars has contributions arising from the presence of a convective envelope. These decay as a power of ω in the limit $\omega \rightarrow 0$, while the overlap integrals of the polytropic model may be shown to decay faster than any power of ω . Note that the overlap integrals for the solar model have also been calculated recently by Weinberg et al (2012). Our calculations for the model 1b agree quite well with their results. It is of interest to note that the overlap integrals for this model are not monotonic at large frequencies. This effect is even more prominent for the models with $M_* = 1.5M_\odot$ and $2M_\odot$ discussed below, where several peaks in the values of \hat{Q} at values of frequencies corresponding to pressure modes are observed, see Figs. 8 and 9. Since this effect is not important for our purposes we do not discuss it

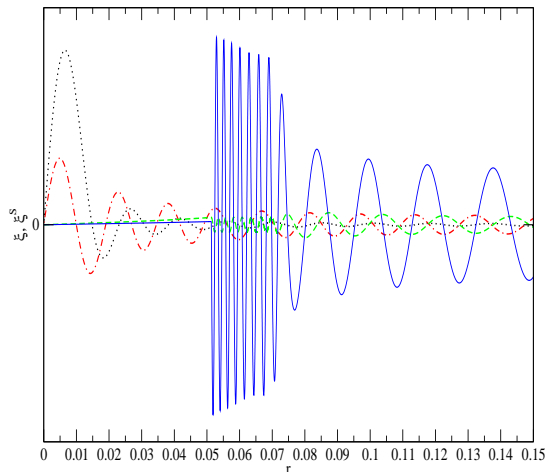


Figure 5. The radial dependence of the radial and tangential components of the displacement vector, ξ and ξ^S , for typical eigenmodes for models 2a and 2d. These are plotted in arbitrary units as functions of the radius r , in the inner region $0 < r < 0.15$. Dotted and dot dashed curves (black and red in the on-line version) and dashed and solid curves (green and blue in the on-line version) show ξ and ξ^S , respectively, for models 2a and 2d. Fig. 2 indicates that model 2a is mostly radiative, while model 2d has a sharp transition from the exterior radiative region to the convective core which is situated at $r_c \sim 0.05$. It is seen that the eigenfunctions corresponding to the mostly radiative model are smooth while those corresponding to the model with a convective core demonstrate a very sharp change of behaviour in the vicinity of $r \sim r_c$.

here. However, we would like to mention that it appears to be rather generic, e.g. it is present in the dependence of \hat{Q} on ω in a model of red giant star, see Fuller et al (2012).

Fig 8 shows results for models 1.5a-1.5c. For the range of frequencies plotted, only model 1.5a has overlap integrals larger than those of the polytrope at small values of ω . As discussed above this is because of the fact that this model has a rather extended convective envelope. From our analytical theory developed in Paper 1, it follows that in the case of model 1.5a, the contribution determined by the presence of this region should be roughly three times smaller than that arising for Sun-like stars. As seen from 8, this is confirmed by our numerical results. More evolved models 1.5b and 1.5c have rather small overlap integrals in the range of frequencies plotted. They are even smaller than those of the polytropic star. This indicates that tidal interactions determined by the excitation of eigenmodes in the shown range of frequencies are relatively weak for these models².

Results for stars of mass $M_* = 2M_\odot$ are shown in Fig. 9. This case is rather similar to the previous one. However, the more massive stars do not have well pronounced convective

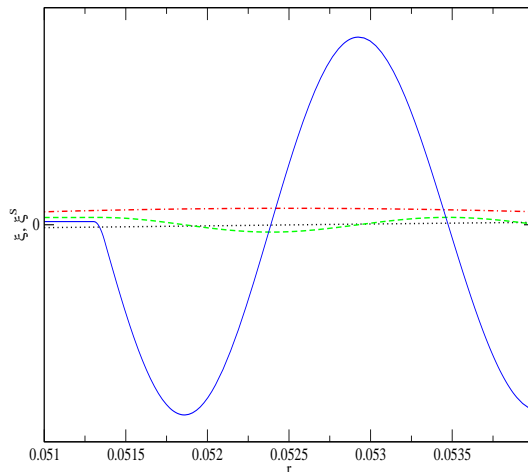


Figure 6. Same as Fig. 5 but a region very close to r_c is shown. One can see that although the eigenfunctions corresponding to model 2d may look discontinuous in Fig. 5, in fact they are smooth.

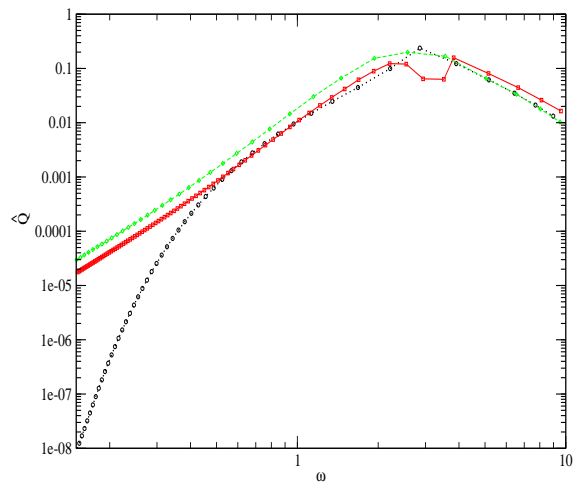


Figure 7. The overlap integrals \hat{Q} as functions of mode eigenfrequency ω for models 1a and 1b plotted with dashed (green in the on-line version) and solid curves (red in the on-line version), respectively. The black dotted curve plots the overlap integrals for a polytrope with $n = 3$. Note that for low frequencies, these are much smaller than the ones corresponding to stellar models with realistic structure. Symbols show the positions of eigenfrequencies, with diamonds, squares and circles representing the results for models 1a, 1b and the polytropic model, respectively. The smooth curves are interpolated through these.

² Note that the strength of tidal interactions also depends on the ratio of the central and stellar mean density, see below

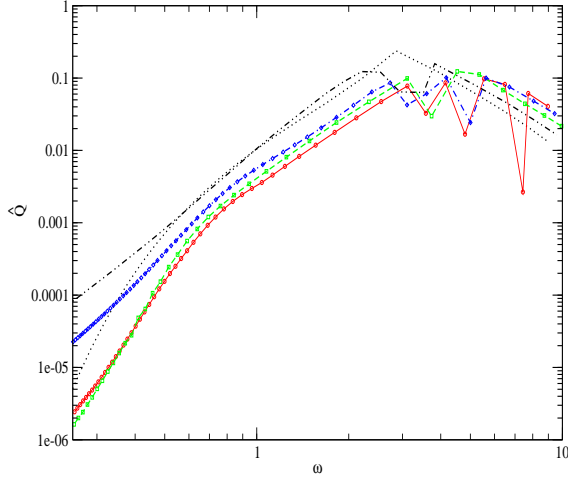


Figure 8. As for Fig. 7 but for models with $M_* = 1.5M_\odot$. Dot dashed (blue in the on-line version), dashed (green in the on-line version) and solid (red in the on-line version) curves are for models 1.5a, 1.5b and 1.5c, respectively. We show the results for models 1p and 1b, plotted as black dotted and dot dot dashed curves respectively, for comparison. Diamonds, squares and circles show positions of particular eigenfrequencies for models 1.5a, 1.5b and 1.5c, respectively.

envelopes and, therefore, their overlap integrals are rather small for the range of frequencies shown, being several times smaller than those for a polytropic star. Finally, in Fig. 10 the overlap integrals of a young star with $M_* = 5M_\odot$ are shown. They are rather similar to, though slightly smaller than those of a polytropic star for the range of frequencies shown. This means that in this frequency range the contribution determined by the presence of a convective core is probably not seen.

3.2 Rotational splitting coefficients

When the rotation frequency of a star, Ω , is small in comparison to its natural frequency: $\Omega \ll \Omega_*$ one may treat effects due rotation in a simplified manner (eg. Lai 1997, Ivanov & Papaloizou 2011). From first order perturbation theory, the eigenfrequencies, ω_j , are shifted with respect to their values for a non-rotating star, $\omega_{0,j}$, by an amount proportional to Ω . We take this shift into account but assume that the overlap integrals are unchanged.

In the inertial frame we have (see eg. Christensen-Dalsgaard 1998)

$$\omega_j = \omega_{0,j} + m\beta_r\Omega, \quad (6)$$

where $m = 0, \pm 1, \pm 2$ is the azimuthal number and β_r are dimensionless coefficients determining the magnitude of the rotational splitting. Note that when the rotation axis is perpendicular to the orbital plane, terms with $m = \pm 1$ do not contribute to the energy and angular momentum transfer as

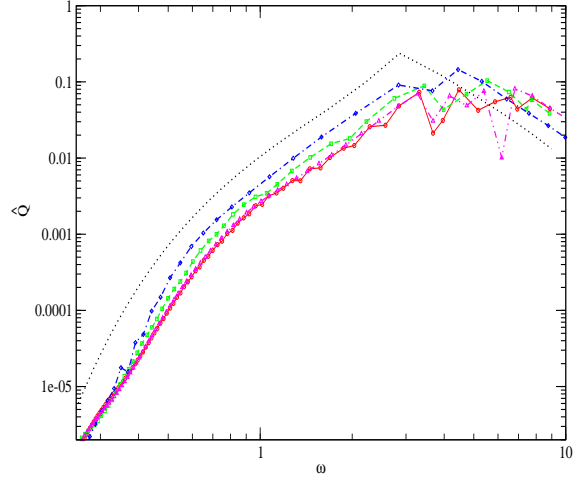


Figure 9. As for Fig. 7 but for models with $M_* = 2M_\odot$. Dot dot dashed (magenta in the on-line version), dot dashed (blue in the on-line version), dashed (green in the on-line version) and solid (red in the on-line version) curves are for models 2a, 2b, 2c and 2d, respectively. Triangles, diamonds, squares and circles show positions of particular eigenfrequencies for models 2a, 2b, 2c and 2d, respectively. The dotted curve gives the results for model 1p.

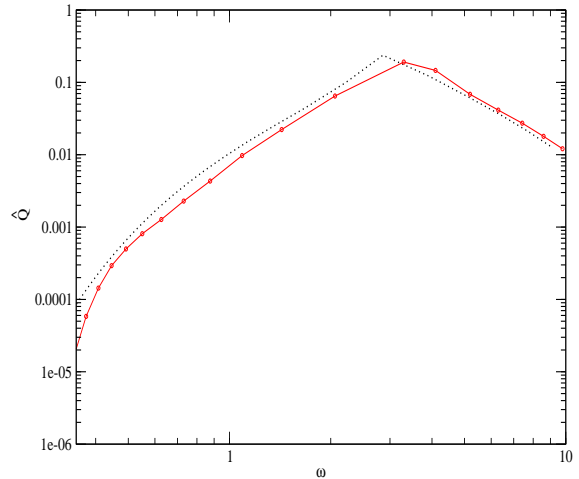


Figure 10. Same as Fig. 7 but for model 5a of a young star with $M_* = 5M_\odot$. The solid (red in the on-line version) curve and circles show the results calculated for this model. The dotted curve is for model 1p.

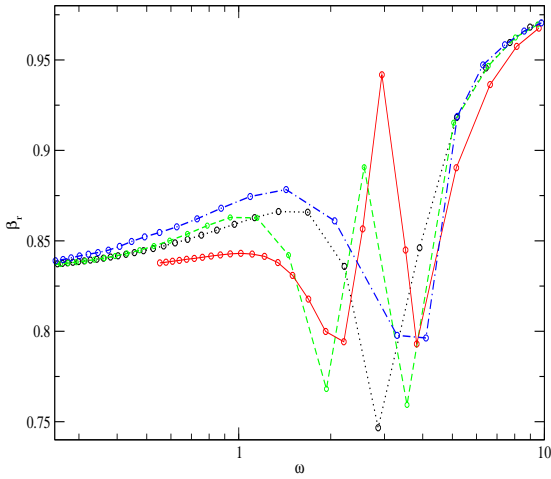


Figure 11. The rotational splitting coefficients β_r as functions of ω for models with $M_* = M_\odot$ and $M_* = 5M_\odot$. Dotted, solid, dashed and dot dashed curves are for models 1p, 1b, 1a and 5a, respectively. Open circles show positions of numerically calculated eigenfrequencies.

a result of a periastron flyby. The rotational splitting coefficients β_r can be expressed as a ratio of two integrals involving the components of the mode Lagrangian displacement. When $\omega_{0,j} \gg 1$ they are close to unity and when $\omega_{0,j} \ll 1$ they tend to $1 - 1/(l(l+1)) = 5/6$ for spherical harmonic index, $l = 2$, (eg. Christensen-Dalsgaard 1998). In the intermediate range of eigenfrequencies these integrals have to be evaluated numerically. We calculate them for our stellar models and illustrate them for models 1p, 1a, 1b and 5a in Fig. 11. Results for models 1.5a - 1.5c are illustrated in Fig. 12, and for models 2a-2d in Fig. 13. One can see from these figures that the dependence of β_r on $\omega_{0,j}$ is not necessarily monotonic, as was also found for the overlap integrals.

From the results presented below, we find that use of the perturbative description of the influence of rotation on tides described above yields results that agree quite well with those obtained from a more accurate approach based on the traditional approximation (Unno et al. 1989), even for quite large stellar angular velocities $\Omega \sim 0.4$. This is the case when either the stellar rotation is retrograde with respect to that of the orbital motion, or prograde with respect to the orbital motion, but with the angular frequency being smaller in magnitude than approximately the value corresponding to pseudosynchronization, for which there is zero angular momentum transfer.

3.3 The overlap integrals in the traditional approximation

As explained in Paper 1 and above, when the traditional approximation is used the overlap integrals \hat{Q} can be represented as products of 'angular' and 'radial' contributions.

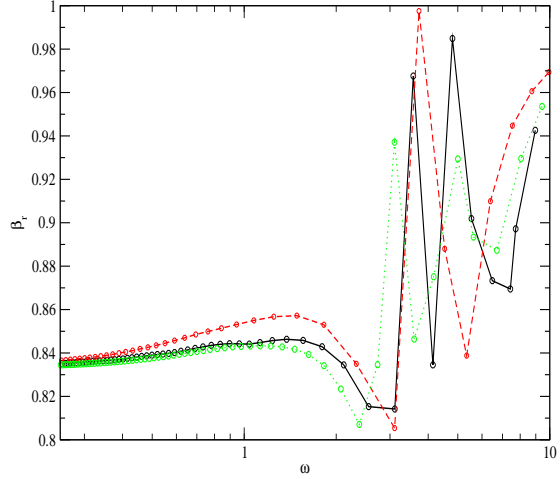


Figure 12. Same as Fig. 11 but for $M_* = 1.5M_\odot$. Solid, dashed and dotted curves are for models 1.5c, 1.5b and 1.5a, respectively.

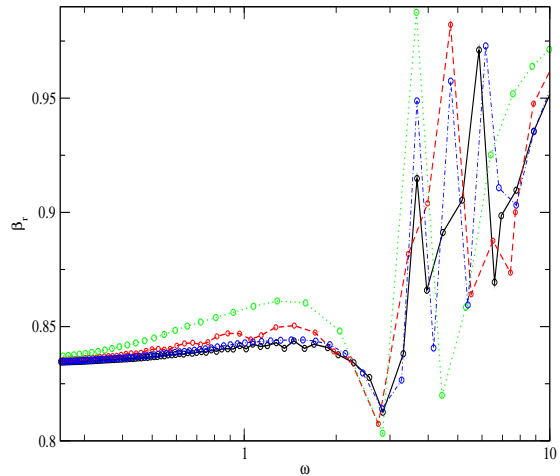


Figure 13. Same as Fig. 11 but for $M_* = 2M_\odot$. Solid, dashed, dotted and dot dashed curves are for models 2d, 2c, 2b and 2a, respectively.

Thus $\hat{Q} = \alpha \hat{Q}_r$, where the angular contribution α is given in Fig. 1 of Paper 1. The radial contribution, \hat{Q}_r , is illustrated in Fig. 14 and 15, for models 1b and 1.5a, respectively. Note that the curves corresponding to the largest retrograde rotation are not monotonic, with the overlap integrals having a pronounced minimum at some value of the eigenfrequency. This effect is explained in Paper 1. Namely, as follows from

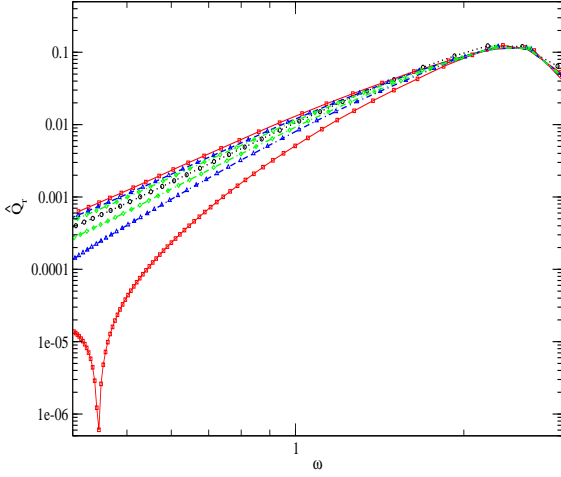


Figure 14. We show the radial contribution to the overlap integrals \hat{Q}_r for model 1b of the present day Sun as functions of eigenfrequency ω for different values of Ω . The cases of $|\Omega| = 0.42, 0.21, 0.11$ and the non-rotating case are shown using solid (red in the on-line version), dashed (blue in the on-line version), dot dashed (green in the on-line version) and black dotted curves, respectively. The curves of the same type with smaller (larger) values of \hat{Q}_r for a given value of ω are calculated for retrograde (prograde) directions of rotation with respect to the pattern rotation associated with the forcing potential. The curves corresponding to the three cases with prograde rotation almost coincide. Symbols show the positions of eigenfrequencies with squares, triangles, diamonds and circles corresponding to $|\Omega| = 0.42, 0.21, 0.11$ and 0 , respectively.

the discussion above, the values of the radial contributions to overlap integrals for stars with extended convective envelopes are mainly determined by contributions coming from the convective envelope and from the vicinity of the base of the convective zone. It can be shown (see Paper 1, equation (111)) that these contributions are proportional to the factor $(1 - 30/\Lambda(\nu))$, where we recall that Λ is the eigenvalue associated with acceptable solutions of the Laplace tidal equation and $\nu = 2\Omega/\omega$. It turns out that in case of retrograde rotation, the value of Λ corresponding to the frequencies, where this minimum is observed, is approximately equal to thirty, and, therefore, the main contributions to the overlap integrals are strongly suppressed.

We use below the traditional approximation described in detail in Paper 1 to calculate the energy and angular momentum transfer for model 1b as a result of a flyby of a perturber on a parabolic orbit for $\Omega = \pm 0.11, \pm 0.21$ and ± 0.42 as well as for model 1.5a for $\Omega = \pm 0.25$ and ± 0.5 . These are compared with results obtained by numerically solving the flyby problem directly as an initial value problem.

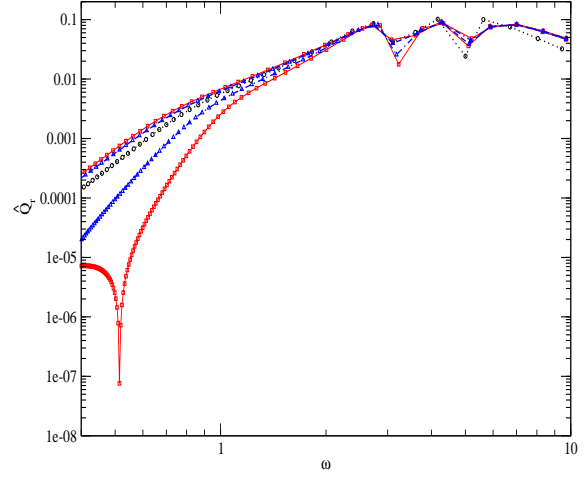


Figure 15. As in Fig. 14 but for model 1.5a. The cases $|\Omega| = 0, 0.25$ and 0.5 are plotted using black dotted, dot dashed (blue in the on-line version) and solid (red in the on-line version) curves, respectively. The curves corresponding to the three cases with prograde rotation almost coincide. Squares, triangles and circles show positions of eigenfrequencies for $|\Omega| = 0.5, 0.25$ and 0 , respectively.

4 TRANSFERS OF ENERGY AND ANGULAR MOMENTUM ARISING FROM PARABOLIC ENCOUNTERS AND THE TIDAL CAPTURE PROBLEM

In this Section we discuss the well known problem of calculating the energy and angular momentum transferred to the normal modes of a star as a result of a parabolic encounter with a perturber treated as a point mass. We consider realistic stellar models. In general, we assume that the stellar rotation axis is perpendicular to the orbital plane. For a discussion of the case of a general inclination between the stellar rotation axis and the orbital angular momentum vector, see Ivanov & Papaloizou (2011).

The magnitude of the energy transferred, ΔE , depends on whether it is calculated in the inertial or rotating frame. In general, we have

$$\Delta E_I = \Delta E + \Omega \Delta L, \quad (7)$$

where ΔE_I and ΔE are the energy transferred as calculated in the inertial and rotating frame, respectively, Ω is the stellar angular velocity, and ΔL is the amount of angular momentum transferred.

It is convenient to introduce natural units for the energy and angular momentum transferred. Thus, we express ΔE_I and ΔE in units of $E_* = Gm_p^2/((1+q)^2 R_*)$, where G is the gravitational constant, m_p is the mass of a perturbing body, and $q = m_p/M_*$. We express ΔL in units of $L_* = q^2(1+q)^{-2} M_* \sqrt{GM_* R_*}$. We remark that all quantities in equations (54) of Paper 1 can also be represented in

natural units³. Once the ratio Ω/Ω_* is specified, the energy and angular momentum transferred expressed in natural units are functions of only one parameter (see eg. Press & Teukolsky 1977, Ivanov & Papaloizou 2004, 2007)

$$\eta = \sqrt{\frac{1}{1+q} \left(\frac{R_p}{R_*}\right)^3} = 3.05\sqrt{\bar{\rho}}P_{orb}, \quad (8)$$

where we recall that R_p is the periastron distance. The quantity $\bar{\rho}$ is the ratio of the mean stellar density to the solar value, $\bar{\rho} = R_\odot^3 M_*/(R_*^3 M_\odot)$, and P_{orb} is orbital period of a circular orbit which has the same value of the orbital angular momentum as the parabolic orbit under consideration, expressed in units of one day.

Assuming that tidal evolution approximately conserves angular momentum (see, eg. Ivanov & Papaloizou (2011) for a discussion of this approximation) P_{orb} characterises the orbital period of the binary system after the process of tidal circularisation is complete. Note that when $q \ll 1$ as for dynamic tides induced in a central star in exoplanetary systems, the condition $\eta = 1$ corresponds to a grazing encounter with periastron distance equal to the stellar radius. Thus, for these systems only $P_{orb} > P_{crit} = 0.325/\sqrt{\bar{\rho}}$ are possible.

We remark that a number of authors (eg. Press & Teukolsky 1977, Lee & Ostriker 1986, Giersz 1986, McMillan, McDermott & Taam 1987) express results in terms of another dimensionless quantity, $T_2(\eta)$ ⁴, which is related to the dimensionless energy transfer, ΔE , through

$$T_2(\eta) = \eta^4 \Delta E. \quad (9)$$

We use equation (9) to compare our results with those obtained by previous authors.

When ΔE_I and ΔE are expressed in natural units, their dependence on η may be used to compare the strength of tidal interactions of stars with different masses and radii. However, for systems with given orbital parameters and m_p it also depends on the average density being larger for stars with smaller $\bar{\rho}$, mainly through the dependence of η on this quantity. Therefore, in a similar way to our previous studies (Ivanov & Papaloizou 2004, 2007, 2011) we introduce the tidal circularisation time

$$T_{ev} = 15 \left(\frac{M_*}{M_\odot}\right) \left(\frac{R_*}{R_\odot}\right) \left(\frac{M_J}{m_p}\right) \frac{1}{\Delta E_I} \sqrt{a_{in}}, \quad (10)$$

where M_J is the mass of Jupiter (see equation (104) of Ivanov & Papaloizou 2007). From here on, it is implied that energy and angular momentum transfers are expressed in natural units, and T_{ev} is expressed in years. Under the assumption that the energy transfers arising from consecutive periastron passages can be simply added, T_{ev} gives a characteristic time scale for the tidal evolution of the semimajor axis of a highly eccentric orbit with initial semi-major axis, a_{in} , in units of 10 AU. We stress that this time scale applies

³ The coefficients A_m should be expressed in units of $GM_p/(R_p^3 \Omega_p)$, where R_p is the periastron distance and a typical periastron passage frequency $\Omega_p = \sqrt{GM_*(1+q)/R_p^3}$. The overlap integral should be in the units of $\sqrt{M_* R_*}$ while the eigenfrequencies and stellar angular frequency are in the units of Ω_*

⁴ We remark that we consider the quadrupole component of the forcing potential.

only to the initial stages of circularisation and will be characteristic of the whole process, only if it can proceed efficiently enough at small eccentricities (see Ivanov & Papaloizou 2011 for a discussion). We set $m_p = M_J$ and $a_{in} = 1$ hereafter, generalisation to other values of m_p simply follows from the form of equation (10).

It is convenient to use equation (10) when considering tidal interactions in systems containing exoplanets. However, dynamic tides may be also important for other problems, such as eg. the tidal capture of stars to form binary systems in stellar clusters (eg. Fabian, Pringle & Rees 1975, Press & Teukolsky 1977). To characterise the strength of tidal interactions in such a setting it is convenient to introduce 'the capture radius' R_{cap} , defined by the condition that when the periastron distance for a tidal encounter between two initially unbound stars is equal to R_{cap} , the initial relative kinetic energy of these stars, when they are very far apart, is equal to the amount of energy transferred due to tidal interactions, i.e.

$$\Delta E_I^{(1)} + \Delta E_I^{(2)} = \frac{1}{2} \frac{M_*^{(1)} M_*^{(2)}}{M_*^{(1)} + M_*^{(2)}} v_{rel}^2, \quad (11)$$

where the upper index, i , denotes quantities associated with star i , and v_{rel} is the initial relative velocity of the stars with respect to each other. Assuming that the binary consists of two identical stars, which rotate in the same sense with respect to their orbital motion, we get

$$\Delta E_I(\eta_{cap}) = 3.125 \cdot 10^{-4} v_*^2, \quad v_* = \sqrt{\left(\frac{M_\odot}{M_*}\right) \left(\frac{R_*}{R_\odot}\right)} \frac{v_{rel}}{10 \text{ km/s}}, \quad (12)$$

and η_{cap} is related to R_{cap} through equation (8) with $R_p = R_{cap}$.

4.1 Energy and angular momentum transfer as a result of a parabolic encounter from direct numerical solution of the linear initial value problem

We have calculated the energy and angular momentum transferred to a star as a result of an encounter with a perturber on a parabolic orbit by solving the linear initial value problem directly. We refer to this procedure as the direct numerical approach. The method adopted follows from that described in Papaloizou & Ivanov (2010) and Ivanov & Papaloizou (2011). The equations solved are (36)-(41) of Ivanov and Papaloizou (2011) with the following modifications. In that work a polytrope of index $n = 3$ and a constant adiabatic index $\gamma = 5/3$ was considered. However, here we consider realistic stellar models for which this varies. Accordingly the quantity $P^{1/\gamma}/\rho \nabla(P'/P^{1/\gamma})$ in equation (36) of Ivanov and Papaloizou (2011) was replaced by $F_{ad}/\rho \nabla(P'/F_{ad})$, where

$$F_{ad} = \int_{P_s}^P \frac{1}{\Gamma_1 P} dP, \quad (13)$$

where $\Gamma_1 = (d \ln P / d \ln \rho)_{adiabatic}$ and P_s is the surface boundary or photospheric pressure. This quantity is readily obtainable for the models provided by numerical integration. Elsewhere in equations (36)-(41) of Ivanov and Papaloizou (2011), γ was replaced by Γ_1 .

The presence of regions with negative $N^2 \equiv \omega_{BV}^2$ gave rise to linearly convectively unstable eigenmodes which would ultimately dominate the solution. In order to remove such modes, as long as the density gradient was negative, we redefined Γ_1 in such regions such that $N^2 \rightarrow 0$ there. This procedure amounts to stating that during linear perturbation, the relationship between P and ρ in these regions is maintained. Here we are adopting the common approximation that the layers are effectively adiabatically stratified (eg. Ogilvie & Lin 2007). This is equivalent to the condition that the convective, or frictional time scale (cf. Zahn 1977) be significantly longer than the rotation period, which is expected to be satisfied for the cases we consider.

In some models, there were small low density regions where the density gradient became positive (see discussion in Section 2.2 above). For these regions, again N^2 was set to zero, but Γ_1 was not allowed to become negative, instead being set to be the largest positive value attained on the grid from the first procedure. In this way an incompressibility condition is approached. However, as the values of the density and pressure were very small, this did not lead to numerical difficulties or, as shown by numerical tests, affect results significantly. As in our previous work, most simulations were carried out on a 200×200 numerical grid with $m = 2$ which gives the dominant contribution. Resolution tests were carried out by doubling the resolution to 400×400 and as in our previous work showed good convergence in these cases with variable Γ_1 .

4.2 Non-rotating stars

In this Section we consider non rotating stars, accordingly $\Omega = 0$. In this case $\Delta E_I = \Delta E$. The results of numerical calculations of ΔE and T_{ev} for the stellar models presented in table 1 are shown in Figs. 16-23.

In Fig 16 we show the dependence of ΔE on η calculated for our models of Sun-like stars, 1a and 1b, together with the same quantities calculated for a polytropic star with solar mass and radius. Circles show results obtained from the direct numerical approach. One can see that the approach based on normal mode calculation gives practically the same energy transfer as the direct numerical approach. A small deviation for $\eta = 8$ are probably due to the effect of numerical diffusion and finite integration time. As seen from Fig.16, the energy transfers for realistic models are significantly larger than those for the polytropic model for large enough values of η . Clearly, this is due to much larger values of the overlap integrals for the realistic models at small eigenfrequencies, see Fig. 7. Interestingly, the energy transfers for models 1a and 1b are quite close to each other regardless of the fact that the overlap integrals corresponding to model 1a are larger than those of model 1b. This is explained by observation that the number of eigenmodes contributing to the tidal interaction is larger in the case of model 1b. This compensates for smaller values of the overlap integrals.

The dot dashed curve shown in Fig. 16 is obtained using the formalism described in paper 1 for model 1b. This curve is calculated by purely analytic means. We see that there is quite good agreement between the analytic and numerical results. In the range $2 < \eta < 10$ the deviation is at most about 40 per cent, when $\eta > 10$, corresponding curves prac-

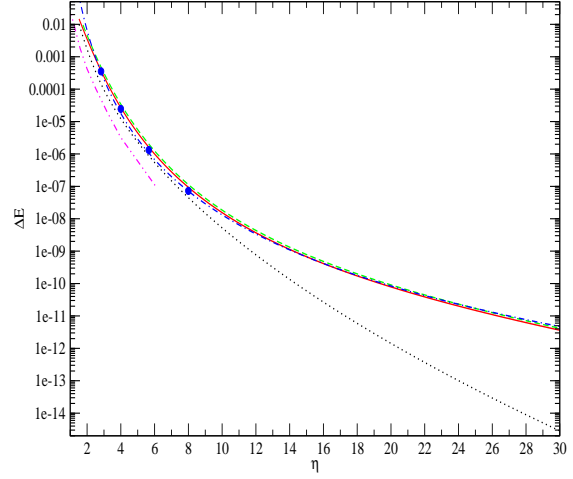


Figure 16. Energy transferred to the normal modes of a non-rotating star with $M_* = M_\odot$ as the result of a parabolic flyby of a perturber of mass $m_p = M_J$, expressed in units of E_* , as a function of the parameter η . The solid, dashed, and dotted curves are for models 1b, 1a and 1p, respectively. The dot dashed curve shows results calculated using the purely analytic expressions for the mode eigenfrequencies and overlap integrals obtained in Paper 1 for model 1b. This almost coincides with the solid line. The dot dot dashed curve shows the result of Giersz (1986). Circles show the energy transfer calculated for model 1b using the direct numerical approach.

tically coincide. The dot dot dashed curve in the same figure shows the result of Giersz (1986) for a solar model. The energy transfer found Giersz (1986) is significantly smaller than we obtain in this paper. Since our results are obtained using three independent methods, we believe that the Giersz (1986) result underestimates the energy transfer, though the origin of the discrepancy is unclear. One possible explanation is that the number of eigenmodes used in his calculation was too small.

From Fig. 17 it follows that the evolution time scale T_{ev} is smaller for model 1b, than for model 1a, for a given value of P_{orb} ⁵. The fact that the model of present day Sun, model 1b, can be tidally excited more efficiently than the corresponding polytropic model, leads to the conclusion that taking into account realistic stellar models can significantly increase estimates of the contribution of tides exerted on the star for the orbital evolution of Jupiter mass exoplanets on highly eccentric orbits. The enhanced tidal interaction can produce a significant change of the orbital semimajor axis in a time of less than $4 \cdot 10^9$ years when $P_{orb} < 4$. Note that this contribution can be further amplified for stars rotating in the opposite sense to that of the orbital motion,

⁵ Note that our calculations for model 1a are not realistic when T_{ev} exceeds its age $\approx 1.7 \cdot 10^8$ years. More realistic calculations of T_{ev} should employ a set of overlap integrals and eigenfrequencies calculated for a grid of stellar models of different ages.

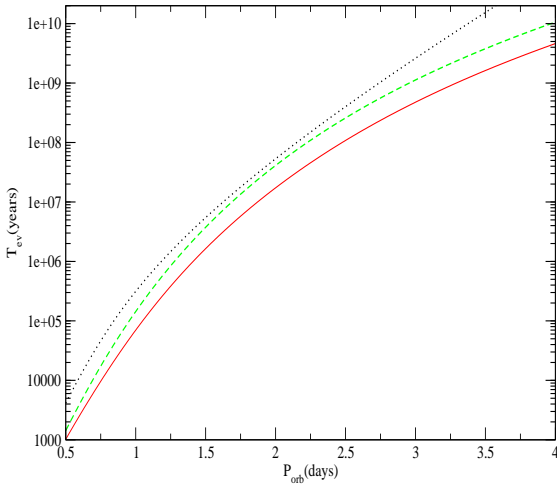


Figure 17. The evolution time T_{ev} as a function of the orbital period after circularisation, P_{orb} , for the same models as illustrated in Fig. 16. Again, the solid, dashed, and dotted curves are for models 1b, 1a and 1p, respectively.

as discussed in Lai (1997), Ivanov & Papaloizou (2011) and below. Furthermore, tides exerted on the star become even more efficient for more massive planets, see eg. Ivanov & Papaloizou (2004), (2007). We also remark that a consequence of the above is that a significant component of the energy liberated by orbital circularisation may be dissipated in the star rather than the planet, thus alleviating the possibility of the potential destruction of the planet (see eg. the discussion in Ivanov & Papaloizou 2004).

In Figs. 18 and 19 we show the energy transfer ΔE and the evolution time T_{ev} calculated for more massive stellar models with $M_* = 1.5M_\odot$. The dotted curves on both Figs. are for our reference models, namely the polytropic model 1p, and the solar model 1b. As seen from Fig. 18 the energy transfer expressed in the natural units is significantly smaller for all the more massive models as compared to the solar model. This is obviously because of the smaller values of the overlap integrals, see Fig. 8. However, at large values of η , model 1.5a gives larger values for the energy transfer than the polytropic model. As discussed above, this is due to the presence of rather extended convective envelope in model 1.5a, which results in larger values of the overlap integrals at small eigenfrequencies as compared to models 1p, 1.5b, and 1.5c.

The symbols in Fig. 18 indicate the energy transfer obtained from the direct numerical approach for models 1.5a and 1.5c. As seen from Fig. 18, the agreement between this method and the normal mode approach is excellent. The dot dashed curve shows the results of McMillan, McDermott & Taam (1987) for a Population II $1.5M_\odot$ star. At sufficiently large values of η , the energy transfer for their model is significantly smaller than that for model 1.5a, but larger than that for models 1.5b and 1.5c. Unfortunately, McMillan, McDer-

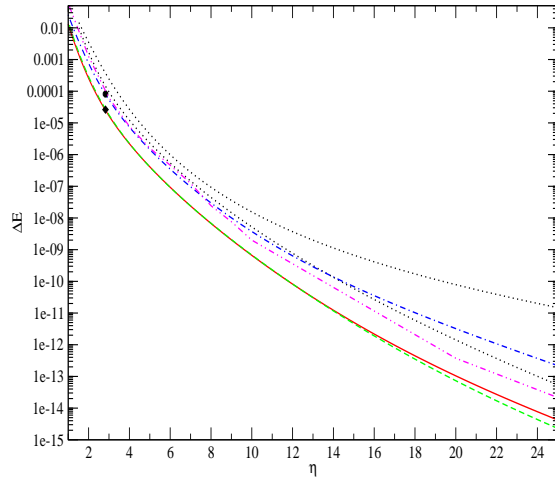


Figure 18. Same as in Fig. 16 but for the models with $M_* = 1.5M_\odot$. The two dotted curves are for our 'reference' models 1p and 1b. The polytropic star, model 1p, has a smaller value of ΔE for a given value of η . Solid, dashed and dot dashed curves are for models 1.5c, 1.5b and 1.5a, respectively. As in Fig. 16, symbols indicate the amount of energy transferred that was obtained adopting the direct numerical approach. The circle and square are for models 1.5a and 1.5c, respectively. The dot dot dashed curve shows the results of McMillan, McDermott & Taam 1987 for a population II model.

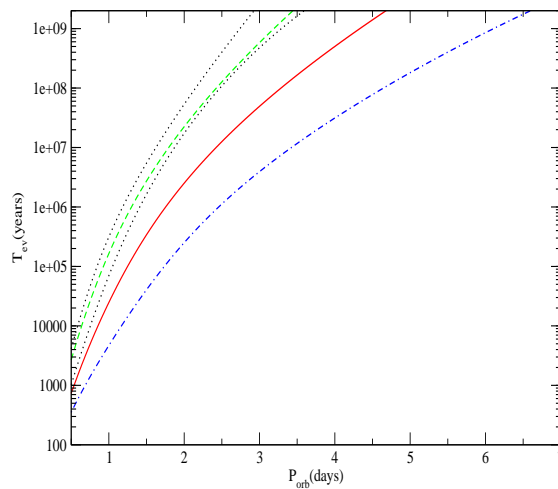


Figure 19. The evolution time T_{ev} for models with $M_* = 1.5M_\odot$ as a function of P_{orb} . Curves of a given type plotted in Fig. 18 and Fig. 19 correspond to the same models.

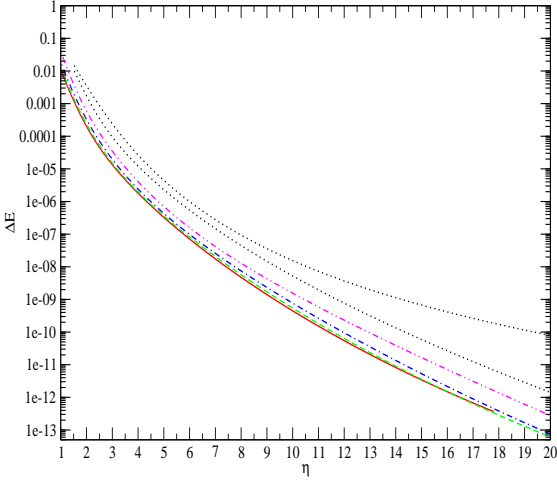


Figure 20. Same as in Fig. 18 but for the models with $M_* = 2M_\odot$. Solid, dashed, dot dashed and dot dot dashed curves are for models 2d, 2c, 2b and 2c respectively, the dotted curves are the same as in Fig. 18.

mott & Taam (1987) did not provide details of their model. Thus it is unclear as to whether this behaviour is a consequence of the form of the Brunt - Väisälä frequency, as is indicated from consideration of our models.

However, it is important to point out that, for a given P_{orb} , the circularisation times, T_{ev} , corresponding to the more massive models are significantly smaller than those for the Sun-like models. This is due to the fact that the mean density of the more massive models is significantly smaller than the mean density of the Sun-like models, see table 1, which leads to smaller values of η for the more massive models for a given value of P_{orb} , see equation (8). In particular, model 1.5c having the largest age $\sim 1.6 \cdot 10^9$ years, has T_{ev} of the order of or smaller than its age, for planets having $P_{orb} < 4$. The increase of the efficiency of the tidal interaction for model 1.5c, as compared to models 1.5b and 1b, can also be viewed as a consequence of the expansion of the star that takes place as a result of evolution.

Models with $M = 2M_\odot$ and $M = 5M_\odot$ are qualitatively similar to models 1.5b and 1.5c. In all cases the energy transfer is even smaller than for the polytropic model, while the evolution times T_{ev} are smaller than those for the reference models 1p and 1b, due to the smaller mean densities of the massive stars. Note that the energy transfers calculated for models 2c and 2d are very close to each other. It is also interesting to note that the value of the mean density evolves non-monotonically with time. For $M_* = 2M_\odot$, model 2d with the greatest age $\sim 10^9$ years, this is smallest. This leads to possibility of significant evolution of the semimajor axis, with $T_{ev} < 10^9$ years, for exoplanets orbiting stars with $M_* = 2M_\odot$ and final orbital periods, assuming the circularisation process can be completed of $P_{orb} < 7$ days, solely due to tides exerted on the star.

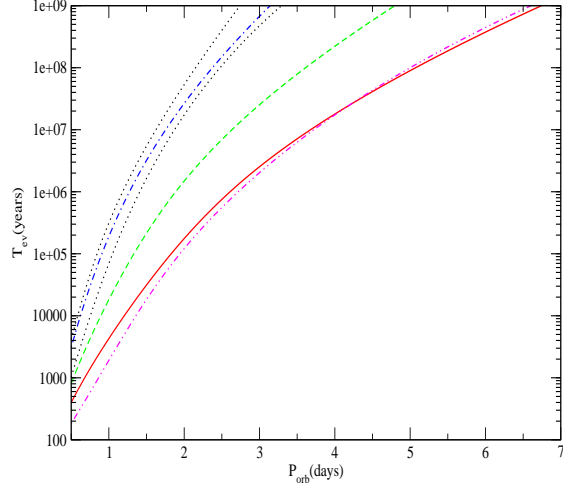


Figure 21. The evolution time T_{ev} for models with $M_* = 2M_\odot$ as a function of P_{orb} . Curves of the same type in Fig. 20 and Fig. 21 correspond to the same models.

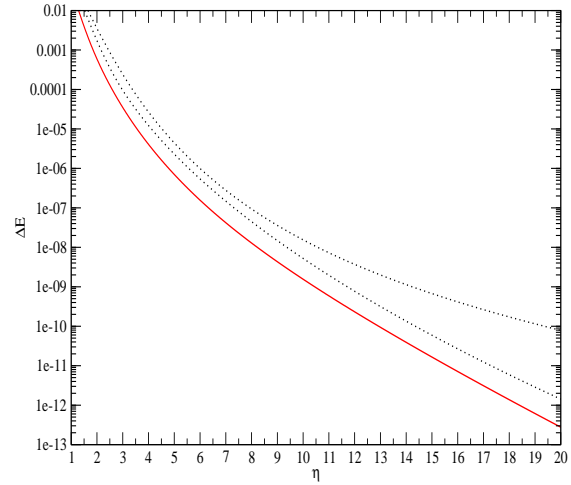


Figure 22. The energy transfer ΔE for the model 5a with $M = 5M_\odot$ shown by the solid curve, the dotted curves show our reference models 1p and 1b as in the previous Figs.

4.3 Rotating stars in the traditional approximation

In this Section we present results for rotating models 1b and 1.5a within the framework of the traditional approximation described in detail in Paper 1. We compare these results to those obtained from the perturbative approach, where it is

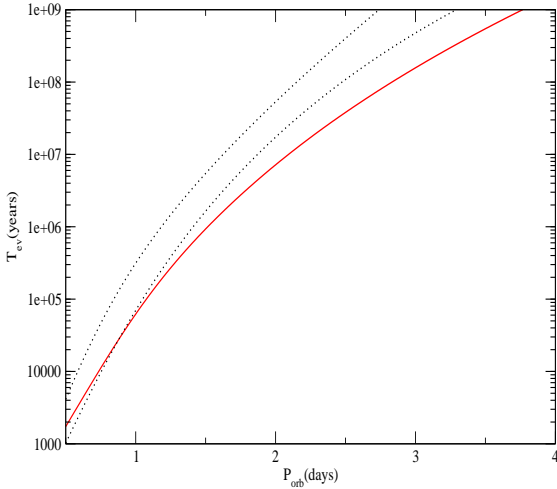


Figure 23. Same as Fig. 22 but for the evolution time T_{ev} .

assumed that the overlap integrals are not changed by rotation, and the mode eigenfrequencies as viewed in the inertial frame are shifted by a factor $m\beta_r\Omega$, as given by equation (6). The perturbative approach is described in more detail in Ivanov & Papaloizou (2011) and references therein. Results are also compared to those obtained following the numerical approach, that is by solving the encounter problem directly as an initial value problem (see section 4.1). In all of this it is assumed that the rotation axis is perpendicular to the orbital plane, with both prograde and retrograde encounters with respect to the direction of the stellar rotation being considered⁶.

4.4 A comparison of eigenspectra obtained from normal mode calculations with those obtained from the direct numerical approach

In order to check whether our direct numerical method and the normal modes approach agree with each other we consider θ -component of the perturbed velocity at a characteristic position in the star as a function of time and make a Fourier transform of the signal. The results are shown in Figs. 24 and 25 for a tidal encounter of a non-rotating star and a retrograde encounter with $\Omega = 0.58$, respectively. In the latter case positive and negative values of the frequency ω correspond to perturbations propagating in the direction of stellar rotation and opposite to this direction, respectively. The value of the amplitude scaling of the Fourier transform is arbitrary. Peaks in these Figs. indicate the approximate positions of free normal mode pulsations. Symbols show the positions of eigenfrequencies calculated using the normal mode approach.

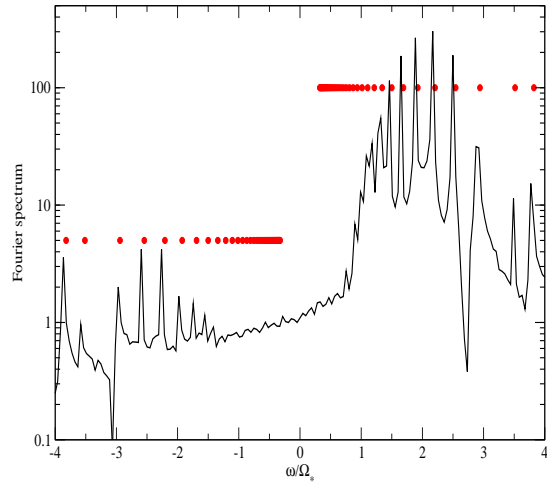


Figure 24. The amplitude of the time Fourier transform of the velocity component in the θ direction evaluated at a characteristic interior point as a function of frequency ω . The case of non-rotating model 1b and $\eta = 4\sqrt{2}$ is presented. Circles show the positions of eigenfrequencies calculated by finding the normal modes, assuming the traditional approximation directly (the normal mode method).

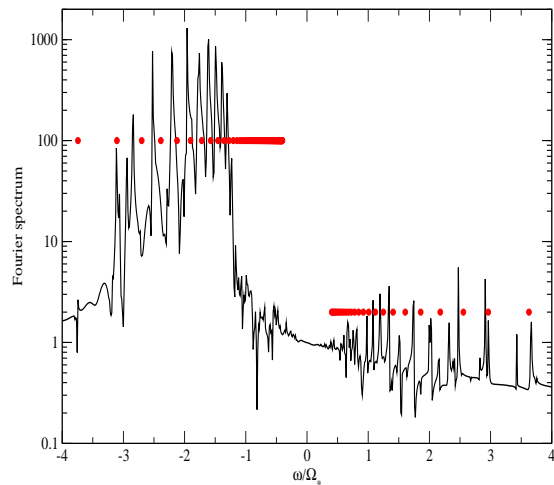


Figure 25. Same as Fig. 24 but for a retrograde tidal encounter with $\Omega = 0.58$.

⁶ For discussion of the general case of an arbitrary inclination of the stellar rotational axis, see Ivanov & Papaloizou (2011).

As seen from Fig. 24, in the case of the non-rotating star, mainly positive eigenfrequencies are excited in the course of tidal encounter. Positions of peaks are in rather good agreement with the normal mode calculations for modes having $|\omega| > 1$. Smaller values of ω are not well resolved on account of the finite time duration of the run.

Contrary to the non-rotating case, the retrograde tidal encounter mainly excites eigenmodes with negative eigenfrequencies, see Fig. 25. Again, the most prominent peaks approximately in the range $-3 < \omega < -1$ are in a rather good agreement with the normal mode method. The eigenfrequencies found from the normal mode method are, however, shifted towards $\omega = 0$ with respect to the positions of the corresponding peaks, the shift being larger for eigenmodes with larger absolute values of ω . The situation is similar for modes with positive values of ω in the range $1 < \omega < 3.5$, but in this case mode eigenvalues are shifted towards larger values of ω with respect to corresponding peak positions. This disagreement is possibly determined by the fact that we use the Cowling and traditional approximations to calculate the eigenspectrum in the normal mode approach. Since smaller absolute values of the eigenfrequencies result in larger values of the associated transfers of energy and angular momentum, we expect that the direct numerical approach gives smaller values of these quantities in the case of retrograde encounters and larger values for prograde encounters. This is indeed obtained in our calculations, see the discussion below. Note too the absence of significant peaks in the inertial range for which $-1.16 < \omega < 1.16$. This is where inertial modes associated with the convective envelope would be expected to show up. However, when confined to a spherical annulus inertial waves may focus on to wave attractors becoming singular in the inviscid limit. Then corresponding discrete inviscid modes may not exist (eg. Ogilvie & Lin 2004, Ogilvie 2013), but instead a continuous spectrum, with the consequence that very prominent resonant spikes are not seen in the response. Nonetheless the relatively small response in the inertial range indicates that inertial waves are not important in this particular case.

4.5 Energy and angular momentum transfer for rotating stars

Figs. 26-30 are for model 1b. In these Figs. we show results obtained from the full numerical approach applied to Sun-like stars having $|\Omega| = 0.42, 0.21, 0.11$ and 0. These are represented by solid, dashed, dot dashed and dotted curves, respectively. In Figs. 26-29 the retrograde encounters have a larger value of the transferred quantity at a given value of η than the prograde encounters. The squares, triangles, diamonds and circles in Figs. 26-28 show the corresponding results obtained using the direct numerical approach, respectively for $|\Omega| = 0.42, 0.21, 0.11$ and 0.

In Fig. 26 we show the transfer of energy in the inertial frame, ΔE , versus η . We see that retrograde encounters always have a larger value of ΔE than prograde encounters, for a given η , with this effect being more extreme for larger absolute values of the angular velocity. The physical reason for this behaviour is discussed in detail in Lai (1997) and Ivanov & Papaloizou (2011). It is interesting to note that prograde encounters with non zero angular velocity produce larger values of ΔE than the case with $\Omega = 0$, when η is

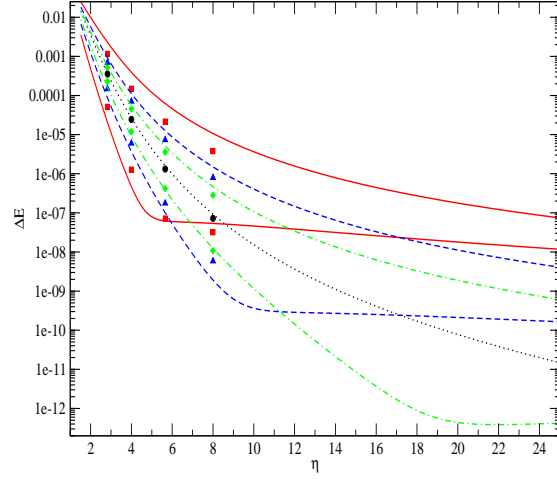


Figure 26. The energy transferred in the rotating frame expressed in natural units as a function of η . Curves of different style correspond to different absolute values of the angular velocity Ω and symbols indicate results obtained using the direct numerical approach. See the text for the allocation of the curves with different styles.

large. Within the framework of rotationally modified gravity modes under the traditional approximation, this is explained by noting that in the limit of very large values of η , the eigenmodes mainly determining the value of ΔE propagate in retrograde direction with respect to the stellar rotation in the rotating frame, but at the same time, they propagate in the prograde direction in the inertial frame, since the pattern speed of these modes is smaller than the angular velocity of rotation. From the results of eg. Ivanov & Papaloizou 2011 it follows that the energy transfer due to these modes is proportional to $\eta^{-2}[\sum_i Q_i^2 I_{2,-2}^2(y)]$, where $y = \eta(2\Omega - |\omega_i|)$, the quantities $I_{l,m}(y)$ are discussed in Press & Teukolsky (1977), see also Ivanov & Papaloizou (2007). The function $I_{2,-2}^2(y)$ has a maximum at $y \approx 2$ and decreases towards smaller and larger values of y . Thus when $y = 1, 3$, it has values approximately one half of its maximum value. Therefore, in order to crudely estimate the energy transfer one may assume that only the contribution of eigenmodes having eigenfrequencies such that $1 < y < 3$ need to be considered and that all these modes have $I_{2,-2}(y) = I_{2,-2}(y = 2)$. The absolute values of the eigenfrequencies are close to $\omega_{max} = 2\Omega - 2/\eta$, being defined by the condition $y(\omega_{max}) = 2$. When $\eta \gg 1$ we can estimate the number of participating modes to be $\propto 1/\eta$. On the other hand, the typical frequency ω_{max} slightly increases when η gets larger, tending asymptotically to 2Ω . For the rotation rates considered in this Paper the overlap integrals corresponding to $\omega_i \approx 2\Omega$ increase quite sharply with increasing ω_i , see Figs. 14 and 15. We have checked that the fact the Q_i increase with increasing η and ω_{max} , approximately compensates for the decrease in the number of modes giving a sizable contribution to ΔE . Therefore, the sum of

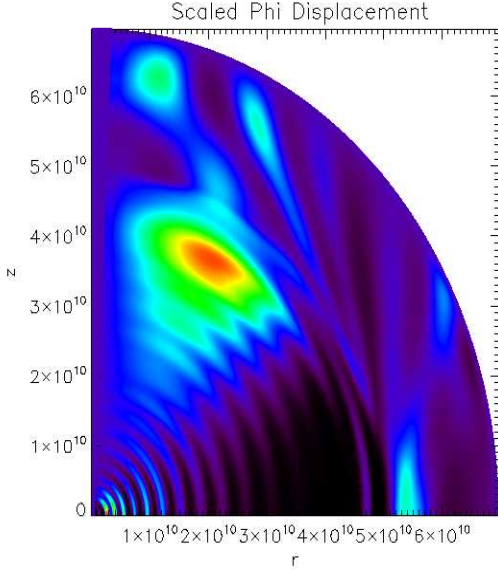


Figure 27. Illustration of inertial waves in the convective envelope for the prograde encounter of model 1b with $\eta = 8$ and $\Omega = 0.21$. Contours of the product of the Lagrangian displacement in the ϕ direction and $\sqrt{\rho}$ are shown in an upper quadrant at a time after the encounter is over and the energy transfer has been completed. The presence of rotationally modified g modes of order up to 15 can be seen in the radiative core while the convective envelope shows the presence of inertial waves that show reflections as well as graze the boundary with the radiative core. The radial coordinate is expressed in cm .

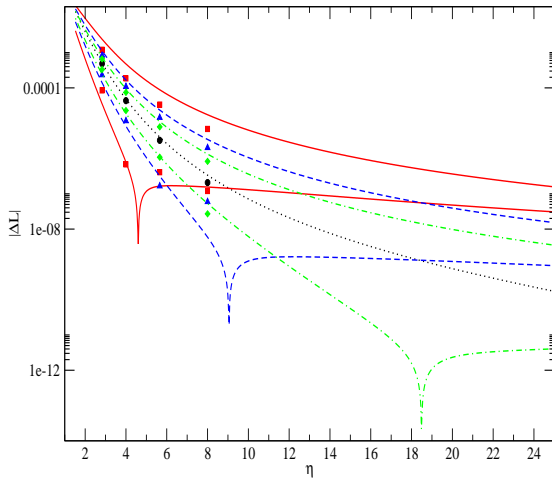


Figure 28. Same as Fig. 26, but for the absolute value of transferred angular momentum, $|\Delta L|$. The locations where ΔL decreases dramatically in magnitude correspond to pseudosynchronization (see text)

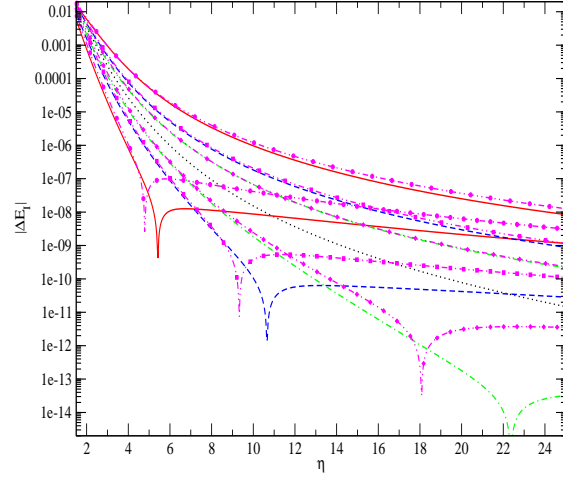


Figure 29. Same as Figs 26 and 28, but for the absolute value of energy in the inertial frame, $|\Delta E_I|$. We recall that ΔE_I is related to ΔE and ΔL through equation (7). Additionally, we show the energy transfer calculated with the framework of the perturbative approach by dot dot dashed lines. Different symbols on these lines correspond to different rotation rates.

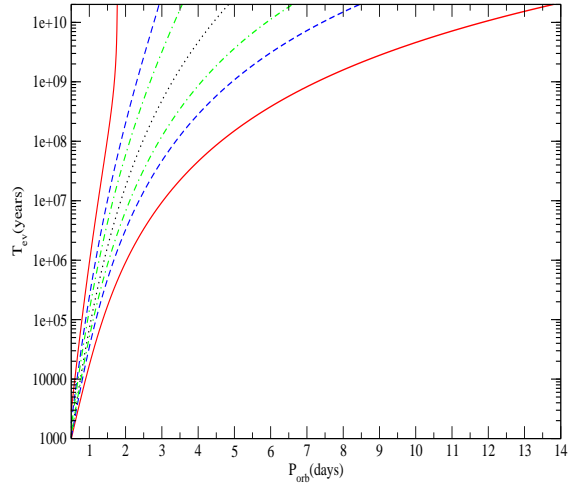


Figure 30. The evolution time T_{ev} defined through equation 10 as a function of the orbital period after circularisation P_{orb} for the rotating solar models. Curves of a given style apply to the same rotation rates as in Fig. 26.

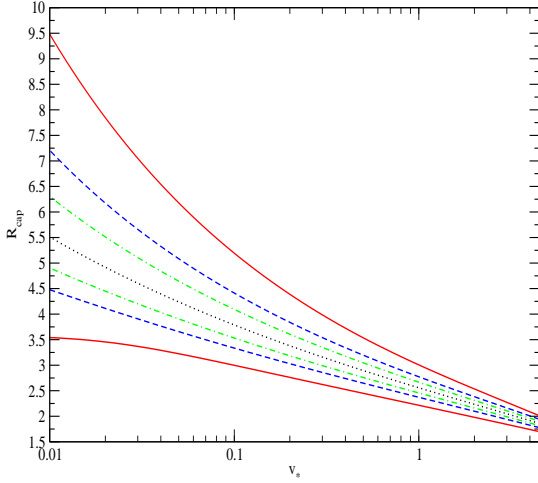


Figure 31. The capture radius R_{cap} calculated according to equation (12) for model 1b as a function of a 'typical' relative velocity v_* . Curves of a given style apply to the same rotation rates as in Fig. 26, with larger values of R_{cap} for a given value of v_* corresponding to retrograde encounters.

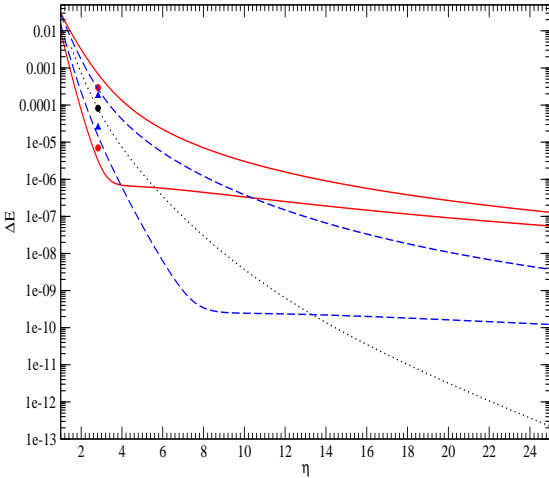


Figure 32. The energy exchange ΔE as a function of η for a rotating model 1.5a. Solid curves and squares, dashed curves and triangles, and finally dotted curves and circles correspond to $|\Omega| = 0.5, 0.25$ and 0 , respectively.

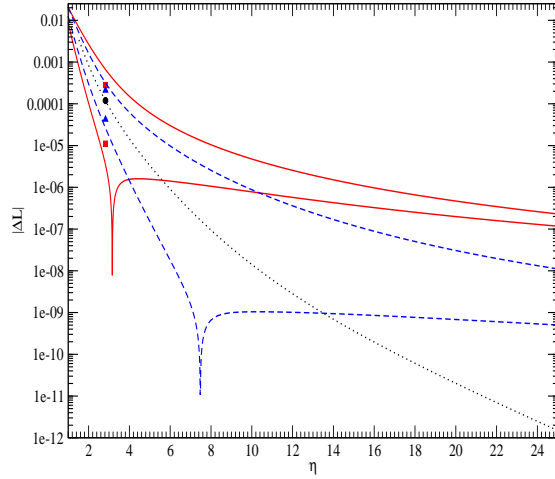


Figure 33. Same as Fig. 32 but the transfer of angular momentum ΔL is shown.

the contributions of these modes behaves approximately as a constant over a range of values of η . In this range $\Delta E \propto \eta^{-2}$ and both ΔE_I and ΔL are negative. Note that this regime persists as long as the number of terms in the sum is larger than one, which corresponds to $\eta < \eta_{max} \approx 2/\Delta\omega$, where $\Delta\omega$ is the distance between two neighbouring eigenfrequencies having $\omega_i \approx \omega_{max}$. When $\eta > \eta_{max}$, ΔE decreases faster than η^{-2} . When $\Omega = 0.42$ we find $\eta_{max} \approx 70$ for the Sun-like models and we have checked that indeed this behaviour is observed in our results.

As discussed above the values of ΔE obtained from the direct numerical approach for the non-rotating star are in excellent agreement with the normal mode method, with only the values corresponding to $\eta = 8$ deviating by about 20%. This deviation may be explained by the influence of numerical viscosity, which leads to relatively more dissipation over the long run times necessary when η is large. Such runs become prohibitive for $\eta > 8$. The case of $\Omega = 0.11$ is quite similar to the non rotating case, with only one sizable deviation of the order of 40% associated with the retrograde encounter with $\eta = 8$. When $\Omega = 0.21$ the deviations are less than 25% for retrograde encounters and less than 30% for prograde encounters with $\eta \leq 4\sqrt{2}$. There is however, a large disagreement for the prograde encounter with $\eta = 8$ for which the direct numerical approach gives ΔE approximately 2.5 times larger than the normal mode method. Convergence checks showed that this discrepancy was not due to lack of numerical convergence of the direct numerical approach.

As seen from Fig. 28, for $\Omega = 0.21$ this η is close to the value where $\Delta L = 0$, where the star is in a state of pseudosynchronization (see e.g. Papaloizou & Ivanov 2005, 2011, Ivanov & Papaloizou 2004, 2007 and references therein). In a similar problem of a tidal encounter of a polytropic rotating star discussed in Papaloizou & Ivanov (2011), an analo-

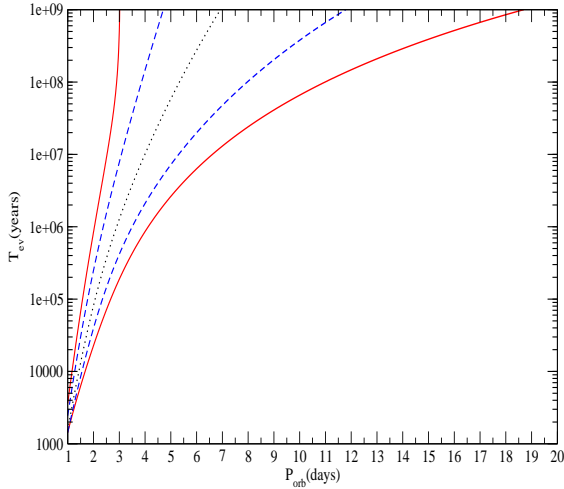


Figure 34. The evolution time scale T_{ev} as a function of the orbital period P_{orb} for model 1.5a. Curves of a given style represent the same rotation rates as in Figs. 32 and 33. For a given absolute value of Ω , the retrograde case corresponds to a smaller value of T_{ev} for a given P_{orb} .

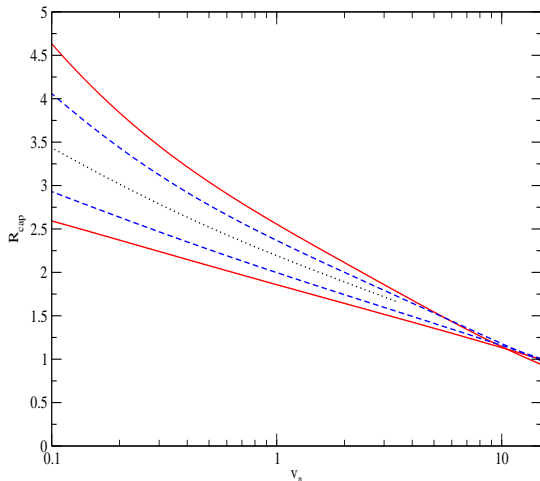


Figure 35. The radius R_{cap} as a function of velocity v_* for rotating 1.5a model. Curves of a given style apply as for Fig. 32. For a given absolute value of Ω , the retrograde case corresponds to a larger value of R_{cap} for a given P_{orb} .

gous disagreement between the direct numerical and normal mode approaches was observed.

Close to the state of pseudosynchronization the normal mode approach indicates that when η is fixed and ΔE and the absolute value of ΔL are considered to be functions of Ω , ΔE has a deep minimum at $\Omega = \Omega_{ps}$, being the value for which pseudosynchronization occurs. At that point $\Delta L = 0$. The differences between the two numerical approaches may result in a shift in the location of this minimum, which because of its depth, causes a large discrepancy when the methods are compared.

In addition, our normal mode approach does not take into account the contribution of inertial waves, which can be excited in the convective regions and increase the amount of transferred energy as viewed in the rotating frame. This effect would be most marked at pseudosynchronization. One would expect that the inclusion of inertial modes would increase ΔE . To estimate the possible magnitude of the effect, we note that Papaloizou & Ivanov (2005) found that for a polytrope with $n = 1.5$,

$$\Delta E = 6.5 \times 10^{-3} E_* / \eta^6. \quad (14)$$

Although only the convective envelope resembles such a polytrope, we use this estimate. In fact there are two corrections, the first arising from the truncation of the envelope at $r \sim 0.7R_*$, is expected to increase ΔE by about an order of magnitude (Ogilvie 2013). The second, due to the fact that the envelope is on top of a more centrally condensed model than the polytrope and so has a lower base density, is expected to decrease ΔE by a similar factor, thus in order to make rough estimates, we simply assume these effects approximately cancel out. Use of (14) for $\eta = 8$, gives $\Delta E \sim 2.5 \times 10^{-8}$ which is about five times the value indicated in Fig. 26. This indicates that inertial modes are likely to be significant under conditions of pseudosynchronization for $\eta = 8$. Similar estimates indicate that is also the case for $\eta > 8$.

In support the above discussion, we comment that the excitation of inertial waves is seen in our simulation of the prograde encounter of model 1b with $\eta = 8$ and $\Omega = 0.21$. To illustrate this, contours of the product of the Lagrangian displacement in the ϕ direction and $\sqrt{\rho}$ are shown in an upper quadrant at a time after the encounter is over and the energy transfer has been completed in Fig. 27. The square of this quantity is proportional to the kinetic energy density of the disturbance associated with motion in the ϕ direction. The presence of rotationally modified g modes is evident in the radiative core. Inertial waves are seen in the convective envelope. These show some reflections and graze the boundary with the radiative core as would be expected for critical latitude phenomena (see Papaloizou & Ivanov 2010).

When $\Omega = 0.42$ the agreement between two approaches is less good. The difference between ΔE is typically a factor of two for the prograde encounters and a factor of three for retrograde encounters at larger η . The fact that such retrograde encounters give a larger disagreement can be explained by the shift of the eigenfrequencies of the dominant excited modes as viewed in the rotating frame. These propagate against the sense of rotation of the star towards larger absolute values as η increases. In this case both the traditional and Cowling approximations used in our normal mode approach become less appropriate.

In Fig. 28 we plot the amount of angular momentum transferred, ΔL , as a function of η . For prograde encounters, in contrast to ΔE , ΔL changes sign at a value of η , where the star rotates at the pseudosynchronization rate. Accordingly, we plot the absolute value of ΔL in this figure. The form of $|\Delta L|$ for prograde encounters is non-monotonic, having a deep minimum for $\eta \equiv \eta_1$, where $\Omega = \Omega_{ps}$. When $\eta < \eta_1$, ΔL is positive (ie. directed in the sense of stellar rotation), on the other hand when $\eta > \eta_1$, it is negative. In the case of retrograde encounters ΔL is always positive (ie. directed in the sense of the orbital motion). The behaviour of the deviation between the direct numerical and normal mode approaches is similar to that found for ΔE . We see again a better agreement for prograde encounters, with the exception of the encounter having $\Omega = 0.21$ and $\eta = 8$, where the deviation is rather large. This may be explained as before.

Overall, our results indicate quantitative agreement between the two approaches when the angular frequency is relatively small, say, $\Omega \leq 0.2$ except for rotation rates close to Ω_{ps} . For faster rotators the agreement is not so good with the direct numerical approach giving values of ΔE that are a factor of 2–3 smaller for retrograde encounters and a factor of 2–3 larger for prograde encounters as long as $\eta < 8$. These discrepancies probably arise from the neglect of inertial waves in the normal mode treatment as well as use of the traditional approximation and the neglect of self-gravity. Excitation of inertial waves would cause ΔE to increase near to pseudosynchronization while the neglect of self-gravity and the use of the traditional approximation become less appropriate for modes excited at the high relative forcing frequencies that occurs for large retrograde stellar rotation.

In Fig. 29 we plot the energy transfer in the inertial frame, ΔE_I related to ΔE and ΔL through equation (7). As for the angular momentum transfer, it is negative for prograde encounters with $\eta > \eta_2$, where $\eta_2 \sim \eta_1$, and, therefore, absolute values are plotted. The energy exchanged for prograde encounters has a sharp minimum at $\eta = \eta_2$, which moves towards larger values of η as the magnitude of Ω decreases. Note that ΔE_I is always positive for retrograde encounters. Let us recall that solid, dashed, dot dashed and dotted curves apply to $|\Omega| = 0.42, 0.21, 0.11$ and 0, respectively. Together with these results we also show the energy transfer calculated adopting the ‘perturbative’ approach where it is assumed that the overlap integrals are not modified by rotation and the eigenfrequencies can be calculated using (6). The respective curves are represented by dot dot dashed lines. Symbols on these lines show different values of $|\Omega|$ with circles, squares and diamonds corresponding to $|\Omega| = 0.42, 0.21, 0.11$, respectively. Remarkably, the perturbative approach agrees quite well with the one based on the traditional approximation, especially for retrograde encounters, even for the largest value of $|\Omega| = 0.42$ adopted. In the case of prograde encounters there is quantitative agreement when $\eta < \eta_2$, and, accordingly, $\Delta E_I > 0$. Since the perturbative approach does not require the calculation of the overlap integrals for every given value of Ω , the evaluation of ΔE_I is simplified to a great extent. It suffices to use the overlap integrals obtained for non-rotating stars together with the frequency splitting coefficients, β_r , given above for a number of stellar models (see eg. Ivanov & Papaloizou 2011).

In Fig. 30 we plot the characteristic timescale of evolu-

tion of the semimajor axis given by equation (10) as a function of P_{orb} . The line styles are as for Fig. 26. It is seen that for a given value of P_{orb} , retrograde encounters have smaller values of T_{ev} than the corresponding prograde encounter. One can see, that for fast rotators, rotation has a significant influence on the strength of tidal encounters (see also Lai 1997 and Ivanov & Papaloizou 2011). For example, when $|\Omega| = 0.11$,⁷ the binary system may significantly change its semimajor axis in less than 10^9 yrs for $P_{orb} < 2.7$ days and < 4 days for prograde and retrograde encounters, respectively. Although stellar rotation significantly slows down in time this effect may contribute to explaining observed exoplanetary systems containing Hot Jupiters with a significant mismatch between directions of their orbital angular momentum and the rotation axis of their central stars.

In Fig. 31 we show the tidal capture radius R_{cap} for the rotating 1b model. As seen from this Fig. the value of R_{cap} is larger for retrograde encounters as compared to prograde encounters as was first noted by Lai (1997). However, this effect is prominent only when either, the rotation rate is quite large, or the characteristic relative velocity, v_* , is small. It is instructive to compare the dependence of R_{cap} on the rotation rate found here with results of Lai (1997), bearing in mind, however, that in that work, a tidal encounter of a $n = 1.5$ polytrope having $M_* = 0.4M_\odot$ and $R_* = 0.5R_\odot$ with a point mass with $m_p = 1.5M_\odot$ was considered. When $v_{rel} = 2.5$ km/s we find $R_{cap} \approx 2.7R_*$ and $4.2R_*$ for prograde and retrograde encounters with the rather large value, $\Omega = 0.42$. On the other hand Lai (1997) gives values of $R_{cap} \approx 4.2R_*$ and $6.4R_*$ for the same encounter, but with $\Omega = 0.6$. The ratio of the radii is approximately 0.65 in both cases. Since the rotation rate of our model is smaller, the relative variation of the capture radius produced by changing from retrograde to prograde rotation is somewhat larger in models of stars with realistic Sun-like structure as expected.

Finally, in Figs. 32–35 we plot the same quantities as in Figs. 26, 28, 30 and 31, but for the rotating model 1.5a. The absolute values of Ω are $|\Omega| = 0.5, 0.25$ and 0. The results behave in a similar way to those found for the rotating Sun-like star, with the difference that the transfers of energy and angular momentum for a given value of η , are smaller for the more massive star, as is found in the non-rotating case. The evolution timescales T_{ev} are, however, larger for the Sun-like star due to its larger average density. For example, model 1.5a with $\Omega = 0.25$ gives an evolution timescale of less than 10^9 years for retrograde encounters, when the orbital period after circularisation $P_{orb} < 12$ days. Of course, as in the previous case, in order to make realistic calculations, one must take into account the evolution of the stellar structure as it affects the mean density of the star, as well as the braking of the stellar rotation with age.

5 CONCLUSIONS AND DISCUSSION

In this paper we have calculated the energy and angular momentum transferred to a number of Population I stellar models with different masses, ages and states of rotation

⁷ This corresponds to a rotation period of the star of approximately one day.

through dynamical tides, as a result of an encounter with a companion on a parabolic orbit. The results were used to estimate the initial evolution time scale of the semimajor axis of a highly eccentric orbit. Complementary methods based on calculation of the normal mode response and a direct numerical approach involving the solution of the encounter problem as an initial value problem were used. These showed quantitative agreement for small and moderate rotation rates $|\Omega| < 0.2$ as long as the distance of closest approach was small enough that the stellar angular velocity is less than the so-called pseudosynchronization frequency.

It was shown that when the energy and angular momentum transferred is expressed in natural units that factor out the dependence on stellar mass and radius so that encounters are characterised by the tidal parameter, η , these quantities depend significantly on the stellar structure. The tidal transfers are significantly larger for models having sufficiently extended convective envelopes. Thus, when $\eta = 8$, other things being equal, the non-rotating 1.5a model undergoes an energy transfer approximately 4 times larger than occurs for models 1.5b and 1.5c, which is explained by the presence of a more extended convective envelope. However, as the solar models 1a and 1b have more extended convective envelopes than models 1.5b and 1.5c which are older than model 1.5a, the energy transferred to them is greater. The effect increases in significance for larger values of η . Thus when $\eta = 8$, it is a factor of 15 times larger.

Since the models of more massive stars with $M_* = 2M_\odot$ and $5M_\odot$ that we considered essentially do not have convective envelopes, the energy transferred to them, expressed in natural units, is rather small. Thus model 5a has a value of ΔE ten times smaller than that for model 1b when $\eta = 8$. Stellar rotation was found to play an important role, with dynamic tides being significantly amplified for retrograde encounters, and weakened for prograde ones, see also Lai (1997) and Ivanov & Papaloizou (2011).

We studied the effect of rotation using the direct numerical approach, the normal mode approach adopting the traditional approximation, and also simply treating the effects of rotation by perturbation theory. In the latter treatment, it was assumed that the overlap integrals are not modified by rotation but that eigenfrequencies are shifted by an amount proportional to the product of the splitting coefficient β_r and rotation frequency Ω , as expected from first order perturbation theory.

It was shown that the perturbative approach gives results in quantitative agreement with the treatment based on the normal mode approach with the traditional approximation, even for fast rotators, as long as the energy transferred in the inertial frame ΔE_I was positive, being approximately equivalent to the condition that the star rotated at less than the pseudosynchronization rate.

As implied by our discussion in section 4.5, this is also the condition for the forcing frequencies to be large enough that the excitation of inertial modes is not expected to play an important role. A condition for this to apply for prograde encounters can be approximately found by requiring that the characteristic forcing frequency, Ω_*/η , exceed 2Ω . Making use of equation (8), we obtain the condition as

$$P_{orb} < \frac{\Omega_*}{6.1\sqrt{\rho}\Omega}, \quad (15)$$

Noting that for a typical rotation period of a T Tauri star of 6 days and solar parameters, equation (15) gives $P_{orb} < 8.4$ days, the implication is that the excitation of stellar inertial modes do not play a significant role in the tidal capture of hot Jupiters into final prograde orbits with periods of a few days.

This simplifies applications of the theory to particular systems since use of the perturbative approach requires only the calculation of the overlap integrals, and the splitting coefficients for a given non rotating stellar model. These are provided for all models considered in this paper. In addition to the methods described above, we also applied the purely analytic approach developed in Paper 1 to the solar model 1b, and showed that it gave results differing from those obtained numerically by at most 40 per cent in the range $2 < \eta < 30$. It is important to stress again that the energy and angular momentum transfers are significantly larger for this model as compared to models of more massive stars and a 'reference' model of $n = 3$ polytrope.

The stellar mean density plays an important role in applications to particular astrophysical systems. This is because tides become relatively more efficient for radially extended low-density objects. In particular, timescale T_{ev} for the evolution of the semimajor axis, considered as a function of the orbital period after the period of circularisation P_{orb} , becomes smaller for more rarefied evolved massive models regardless of the fact that other effects, such as possessing a smaller convective envelope, act in the direction of making tidal interaction less efficient as discussed above. Thus, T_{ev} is less than 10^9 yrs for non-rotating models 1b and 1.5c when $P_{orb} < 3.3$ days and < 4.3 days, respectively. For fast rotators this time can be significantly reduced for retrograde encounters. Thus, in the case of a 1.5a model rotating with the angular frequency $\Omega = 0.25 T_{ev} < 10^9$ yrs when $P_{orb} < 12$ days.

When the theory of dynamic tides is applied to particular astrophysical processes, such as the tidal circularisation of exoplanet orbits starting with a high eccentricity induced by gravitational scattering, or the process of tidal capture of stars in stellar clusters, it is important to calculate the overlap integrals and the coefficients β_r for a grid of stellar models of different ages. It is also important to understand the evolution of the stellar structure, and rotation rate as a function of time. The outcome of tidal evolution may differ significantly for stars with different masses and different rotational history.

As discussed in Paper 1 the overlap integrals are also important for discussing the tidal evolution of binaries with small orbital eccentricity. In particular, for forcing frequencies large enough that inertial modes are not expected to be excited, they fully determine the effect of tidal interactions in the regime of 'moderately large viscosity', see eg. Goodman & Dickson 1998 and Paper 1. The results of Zahn (1977) can only be recovered only when the overlap integrals are $\propto \omega^{17/6}$. This dependence approximately holds for Sun-like stars in the limit of $\omega \rightarrow 0$. It is determined by the functional form of the square of the Brunt-Väisälä frequency in the neighbourhood of the transition from radiative to convective regions. In particular the $\omega^{17/6}$ dependence of the overlap integrals requires that, in the neighbourhood of the transition, the square of the Brunt-Väisälä frequency is a linear function of the difference between a given radius and the radius of the transition. This assumption may not

be valid for a massive star, where the transition from the radiative envelope to the convective core can be extremely sharp. In particular, the Zahn (1977) theory does not apply to binaries with ultra-short periods $P_{orb} \sim 10\Omega_*^{-1}$, where the overlap integrals decrease much faster with ω , see the discussion of Figs. 7-10 in the text. A theory appropriate for large orbital periods must consider the origin of, and take into account, possible rapid variations of the the Brunt-Väisälä frequency in the neighbourhood of the convective to radiative transition. This is left for future work.

ACKNOWLEDGEMENTS

We are grateful to I. W. Roxburgh for providing stellar models and he and G. I. Ogilvie for fruitful discussions. We also thank S. V. Vorontsov for useful comments.

PBI and SVCh were supported in part by Federal programme "Scientific personnel" contract 8422, by RFBR grant 11-02-00244-a, by grant no. NSH 2915.2012.2 from the President of Russia and by programme 22 of the Presidium of Russian Academy of Sciences.

Additionally, PBI was supported in part by the Dynasty Foundation and thanks DAMTP, University of Cambridge for hospitality.

REFERENCES

- Christensen-Dalsgaard, J., Dappen, W., Ajukov, S. V., Anderson, E. R., Antia, H. M., Basu, S., Baturin, V. A., Berthomieu, G., Chaboyer, B., Chitre, S. M., Cox, A. N., Demarque, P., Donatowicz, J., Dziembowski, W. A., Gabriel, M., Gough, D. O., Guenther, D. B., Guzik, J. A., Harvey, J. W., Hill, F., Houdek, G., Iglesias, C. A., Kosovichev, A. G., Leibacher, J. W., Morel, P., Proffitt, C. R., Provost, J., Reiter, J., Rhodes Jr., E. J., Rogers, F. J., Roxburgh, I. W., Thompson, M. J., Ulrich, R. K., 1996, *Science*, 272, 1286 - 1292
- Christensen-Dalsgaard, J., 1998, *Lecture Notes on Stellar Oscillations*, 4th Edition, <http://users-physics.au.dk/jcd/oscilnotes/>
- Eggleton, P., 1972, *MNRAS*, 156, 361
- Fabian, A. C., Pringle, J. E., Rees, M. J., 1975, *MNRAS*, 172, 15P
- Fuller, J., Derekas, A., Borkovits, T., Huber, D., Bedding, T., Kiss, L., 2012, *arXiv:1211.6814*
- Giersz, M., *Acta Astronomica*, 1987, 36, 181
- Goodman, J., Dickson, E. S., 1998, *ApJ*, 507, 938
- Hut, P., 1981, *A&A*, 99, 126
- Ivanov, P. B., Papaloizou, J. C. B., 2004, *MNRAS*, 347, 437
- Ivanov, P. B., Papaloizou, J. C. B., 2007, *MNRAS*, 376, 682
- Ivanov, P. B., Papaloizou, J. C. B., 2011, *Celestial Mechanics and Dynamical Astronomy*, 111, 51
- Ivanov, P. B., Papaloizou, J. C. B., Chernov, S. V., 2013, *MNRAS*, 432, 2339 (Paper 1)
- Kippenhahn, R., Weigert, A., Weiss, A., 2013, *Stellar structure and Evolution: Astronomy and Astrophysics Library*, ISBN 978-3-642-30255-8. Springer-Verlag Berlin Heidelberg
- Lai, D., 1997, *ApJ*, 490, 847
- Latour, J., 1970, *A&A*, 9, 277
- Lee, H. M., Ostriker, J. P., 1986, *ApJ*, 310, 176
- McMillan, S. L. W., McDermott, P. N., Taam, R. E., *ApJ*, 1987, 36, 181
- Ogilvie, G. I., Lin, D. N. C., 2007, *ApJ*, 661, 1180
- Ogilvie, G. I., 2013, *MNRAS*, 429, 613
- Papaloizou, J. C. B., Ivanov, P. B., 2005, *MNRAS*, 364, L66
- Papaloizou, J. C. B., Ivanov, P. B., 2010, *MNRAS*, 407, 1631
- Press, W. H., Teukolsky, S. A., 1977, *ApJ*, 213, 183
- Rasio, F. A., Ford, E. B., 1996, *Science*, 274, 954
- Roxburgh, I. W., 1978, *A&A*, 65, 281
- Roxburgh, I. W., 2008, *Astrophysics and Space Science*, 316, 75
- Silva Aguirre, V., Ballot, J., Serenelli, A. M., Weiss, A., 2011, *A&A*, 529, 63
- Unno, W., Osaki, Y., Ando, H., Saio, H., Shibahashi, H., 1989, "Nonradial oscillations of stars", Tokyo: University of Tokyo Press, 2nd ed.
- Weidenschilling, S. J., Marzari, F., 1996, *Nature*, 384, 619
- Weinberg, N. N., Arras, P., Quataert, E., Burkart, J., *ApJ*, 2012, 751, 136
- Zahn, J.-P., 1977, *A&A*, 57, 383
- Zahn, J.-P., 1991, *A&A*, 252, 179